# A NOVEL SHAPE FEATURE TO CLASSIFY MICROCALCIFICATIONS

By

Yiming Ma

A Thesis
Submitted to the
Faculty of the Graduate School
of
Western Carolina University
in Partial Fulfillment of
the Requirements for the Degree
of
Master of Science

Committee:

_____ Director

_____

_____

_____ Dean of the Graduate School

Date: _____

Spring 2010
Western Carolina University
Cullowhee, North Carolina

# A NOVEL SHAPE FEATURE TO CLASSIFY MICROCALCIFICATIONS

A thesis presented to the faculty of the Graduate School of Western Carolina University in partial fulfillment of the requirements for the degree of Master of Science.

By

Yiming Ma

Director: Peter C. Tay, PhD
Assistant Professor
Department of Engineering and Technology

March 2010

This thesis is dedicated to my parents.

ACKNOWLEDGEMENTS

Dr. Peter C. Tay has been the ideal advisor. Without his sage advice for the research and patient criticism on composing final paper, this thesis would not have been possible.

I am grateful for having Dr. James Z. Zhang and Dr. Robert D. Adams as my committee member and their generous help in every aspect during the past two years.

Lastly, I offer my regards and blessings to all of my friends and classmates who supported me in any respect during the completion of the project.

TABLE OF CONTENTS

LIST OF TABLES

LIST OF FIGURES

# ABSTRACT

A NOVEL SHAPE FEATURE TO CLASSIFY MICROCALCIFICATIONS

Yiming Ma, M.S.T.

Western Carolina University (March 2010)

Director: Peter C. Tay, PhD

Clinical evident shows that the shape of mammographic calcification is an indicator of the pathology. Microcalcifications (MC) with rough shape are early signs of malignant breast cancer. This thesis proposed a shape metric to help radiologist in classifying regions of interest. Region growing and gradient vector flow algorithm are used to obtain the contour of MC to calculate the normalized distance signature. A three level wavelet decomposition with a Daubechies eight tap wavelet is used to provide a bandpass function and extract the desired shape feature of the MC. A comparison with previously used shape features such as compactness, moment, Fourier descriptors is provided. 58 malignant and 125 benign cases, totaling 368 individual MC, are tested by the proposed method and previously used shape features.

# CHAPTER 1: INTRODUCTION

In 2006 cancer was reported as the second leading cause of death in the United States with 559,888 cases, which is equivalent to 23.1% of total deaths [2].[1] In [3], the American Cancer Society (ACS) reported that breast cancer is the most common cancer among women, accounting for nearly 1 in 4 cancers diagnosed in US women.[2] Table. 1.1 shows ACS's most recent estimates [3] for breast cancer in the United States for 2009[3]:

Table 1.1: Estimated New Female Breast Cancer Cases and Deaths by Age, US, 2009

| Age | In Situ Case | Invasive Cases | Deaths |
|---|---|---|---|
| Younger than 45 | 6,460 | 18,640 | 2,820 |
| 45 and older | 55,820 | 173,730 | 37,350 |
| Younger than 55 | 24,450 | 62,520 | 8,890 |
| 55 and older | 37,830 | 129,850 | 31,280 |
| Younger than 65 | 40,940 | 120,540 | 17,200 |
| 65 and older | 21,340 | 71,830 | 22,970 |
| All Age | 62,280 | 192,370 | 40,170 |

It is widely accepted that early detection tests for breast cancer can save many thousands of lives each year [4]. Mammography and palpation are the two conventional ways to screen for breast cancer. Mammography is the process of using X-rays radiation to examine the human breast and is used as a diagnostic as well as a screening tool. The

[1] Heart disease is listed as the leading cause with 631,636 cases, which is equivalent to 26.0% of total deaths in [2].

[2] Men are generally at low risk for developing breast cancer

[3] Rounded to the nearest 10

presence of clusters of microcalcifications (MC), which are at least three tiny deposits of calcium within a one $cm^2$ region, could provide information for experienced radiologist to detect the early sign of breast cancer [5]. MC generally have a diameter from 0.1mm to 0.5mm and are hard to detect, especially in dense parenchynmal tissue. The presence of MC or MC cluster does not necessarily indicate the presence of malignant cancer. Radiologists evaluate the shape, morphology, and pattern of clusters of MC to determine if a biopsy is warranted.

This paper presents a method to extract a new shape feature from MC found in mammography. The background of computer-aided-analysis and previous work are discussed in Chapter 2; the proposed method is presented in detail in Chapter 3; a comparison of the proposed method with the previous classifier is presented in Chapter 4. Chapter 5 presents a conclusion.

# CHAPTER 2: LITERATURE SURVEY

There are variety of proposed methods to classify mammographic region of interests (ROIs). A summary of previous methods used in various stages of computer-aided diagnosis (CAD) are provided. Although the following is not a fully inclusive list, the described features represent a wide range of MC characteristics. Several features such as Haralick features, wavelet features, multi-wavelet features and shape feature [1] are developed as classifier for MC and MC cluster. Individual MC features, statistical texture features, multi-scale texture features as well as fractal dimension features are used in detecting MC [6]. Segmentation process usually takes place together with or after successful detection. The purpose of segmentation is to separate certain featured parts from each other and the background of an image and to divide those into non-overlapping regions. The two main reasons for MC segmentation are to obtain the location of MC to assist radiologists and to classify the abnormalities into benign and malignant categories [7].

In mammography analysis, the background is not uniformly changing due to the non-uniformity of the density of breast tissue. Therefore segmentation of MC usually demands an adaptive method. MC usually appear brighter than its background. If a local threshold method is used to detect MC, then a threshold value for a sub-image and a selection of window size are required. Arikidis et al. present a size-adapted MC segmentation by applying a multiple scale active contour, which is initialized by active ray [8]. Other methods such as non-linear filter, wavelet transform [9] active contour [10] and neutral network [11] have also been proposed. Also in [12, 13], the authors proposed another approach to CAD

mammography by detecting a whole MC cluster rather than a single MC.

## 2.1 Haralick Feature

The Haralick feature analysis [14,15] is known as the spatial gray-level dependence method. This method has previously been used for MC classification in MRI images. The basis for these features is the gray-level co-occurrence matrix H given by

$$\mathbf{H} = \begin{bmatrix} P(1,1) & P(1,2) & \dots & P(1,N_0) \\ P(2,1) & P(2,2) & \dots & P(2,N_0) \\ \vdots & \vdots & \ddots & \vdots \\ P(N_0,1) & P(N_0,2) & \dots & P(N_0,N_0) \end{bmatrix}. \tag{2.1}$$

where $P(i,j)$ is defined as the number of $i^{\text{th}}$ pixel values that are adjacent to the $j^{\text{th}}$ pixel

Table 2.1: Table of Haralick features

| | |
|---|---|
| Angular Second Moment | Contrast |
| Corelation | Sum of Squares: Variance |
| Inverse Difference Moment | Sum Average |
| Sum Variance | Sum Entropy |
| Entropy | Difference Variance |
| Difference Entropy | Info. Measure of Correlation 1 |
| Info. Measure of Correlation 2 | Max. Correlation Coefficient |

value, divided by the total number of such comparisons. The dimension of this matrix is $N_0 \times N_0$, where $N_0$ is the number of gray levels in the image. Each entry represents the probability that an $i^{\text{th}}$ pixel value is adjacent to a $j^{\text{th}}$ pixel value. Based on this gray-level co-occurrence matrix **H**, Haralick generated 14 texture features listed in Table 2.1.

## 2.2 Wavelet Feature

Another widely used method is analyzing an image in multi-scale resolution. In [16], a general paradigm for the analysis and application of discrete multiwavelet transforms

is provided. Wavelet analysis is a powerful tool to achieve multi-scale resoloution. A computer-aided method to overcome the two main difficulties of detecting MC, which are low contrast between MC and its background and high false positive rate in MC classification, is provided in [17] with applying wavelet to remove the background noise and Markov random field to enhance the recognition of MC.

The extraction of wavelet feature is based on decomposing the image and calculating the entropy and energy of each sub-bands. In a $N \times N$ sub-image, normalized energy and entropy are computed as [1]:

$$normalized\ energy = \frac{\sum_i \sum_j x_{ij}}{N^2} \tag{2.2}$$

$$normalized\ entropy = -\frac{\sum_i \sum_j \left[\frac{x_{ij}^2}{P^2}\right] log_2 \left[\frac{x_{ij}^2}{P^2}\right]}{log_2 N^2} \tag{2.3}$$

where $x_{ij}$ is the $i^{\text{th}}$, $j^{\text{th}}$ pixel value of the sub-images, and

$$P^2 = \sum_i \sum_j x_{ij}^2 \, . \tag{2.4}$$

## 2.3 Shape Feature

In [18], the authors proposed a combination of three shape features of individual MC shape and claimed a 100% accuracy of detection by applying a nearest-neighbor method classifier. The mathematical expressions of these three features are:

1. Compactness

$$C = \frac{P^2}{A} \tag{2.5}$$

where $P$ is the length of region perimeter and $A$ is the area of the MC.

2. Moment $F_3 - F_1$

   Given $z(i)$, $i = 1, 2, ..., N$ are the Euclidean distances of the ordered contour pixels to the reference (centroid) point and $N$ is the number of contour pixels, the $p^{\text{th}}$ moment is defined as

$$m_p = \frac{1}{N} \sum_{i=1}^{N} |z(i)|^p \ . \tag{2.6}$$

   The $p^{\text{th}}$ central moment is defined as

$$M_p = \frac{1}{N} \sum_{i=1}^{N} |z(i) - m_1|^p \ , \tag{2.7}$$

   The $F_3 - F_1$ feature is used as the shape feature for classifying MC and is defined as

$$F_3 - F_1 = \frac{M_4^{\frac{1}{4}}}{m_1} - \frac{M_2^{\frac{1}{2}}}{m_1} \ . \tag{2.8}$$

3. Fourier Descriptor

   The Fourier Descriptor is computed by representing each pixel by a complex number $Z_i = x_i + jy_i$, where $x_i$ and $y_i$ are the coordinate of each pixels. The Fourier descriptors are defined as:

$$A(n) = \frac{1}{N} \sum_{i=0}^{N-1} Z_i e^{-j\frac{2\pi}{N}ni} \ . \tag{2.9}$$

   To make the Fourier descriptor invariant to position, size, orientation and starting point of the contour, the Fourier Descriptor is normalized as:

$$NFD(k) = \begin{cases} 0 & k = 0 \\ A(k)/A(1) & k = 1, 2, ..., N/2 \\ A(k+N)/A(1) & k = -1, -2, ..., -N/2+1 \end{cases} \ . \tag{2.10}$$

   The feature FF (Fourier Feature) is defined based on the NFD as:

$$FF = \frac{\sum_{k=-N/2+1}^{N/2} \|NFD(k)\|/|k|}{\sum_{k=-N/2+1}^{N/2} \|NFD(k)\|} \ . \tag{2.11}$$

   where $\|NFD(k)\|$ denotes the magnitude of $NFD(k)$.

## 2.4 Other Features

Table 2.2: Table of shape features provided in [1]

| | |
|---|---|
| 1 | Number of microcalcifications in cluster |
| 2 | Maximum size of microcalcifications in cluster |
| 3 | Standard deviation of the size of microcalcifications in cluster |
| 4 | Number of microcalcifications with size of one pixel |
| 5 | Sum of the area of the microcalcifications in each cluster |
| 6 | Maximum value of compactness in cluster |
| 7 | Average compactness in cluster |
| 8 | Maximum value of F3-F1 in cluster |
| 9 | Average value of F3 in cluster |
| 10 | Maximum value of F3 in cluster |
| 11 | Average F3 in cluster |
| 12 | Radius of the circle that best fits the cluster |
| 13 | Scattering of the microcalcifications |
| 14 | Average gray level of the microcalcifications in cluster |
| 15 | Standard deviation of the mean of the microcalcification gray levels in the cluster |
| 16 | Maximum standard deviation of the gray levels in each microcalcification |
| 17 | Average standard deviation of the gray levels in each calcification in cluster |

The features described in this chapter are not a fully complete list. The reader is referred to [1] for a more comprehensive description of the proposed MC feature listed in Table 2.2.

# CHAPTER 3: METHODOLOGY

This chapter provides detailed information about the proposed method to classify benign and malignant cases by analyzing the MC shape feature. Firstly, the definition and attribute of the distance signature are introduced. Secondly, explanation of why and how I implemented the algorithm is presented. Finally, the flow chart of the complete method is given in Fig 3.7.

## 3.1 Region Growing Algorithm

The region growing method (RGM) is adopted to segment MC in my proposed method. The RGM starts from a user specified seed point with a chosen tolerance $(0 \leq \tau \leq 1$, typically $\tau = 0.025)$. Initially, the seed point is the only point of a region. A neighboring point value $p(i, j)$ of a region is added to the region if the following criteria is satisfied:

$$(1-\tau)\frac{(P_{max}+P_{min})}{2} \leq p(i,j) \leq (1+\tau)\frac{(P_{max}+P_{min})}{2} \tag{3.1}$$

where $P_{max}$ and $P_{min}$ is the maximum and minimum value of the current region and $\tau$ is a predefined tolerance. Each iteration grows the region until a maximum number of iterations is performed. The maximum search iteration in my proposed method is set to 500. It has been empirically verified that this depth is sufficient enough for the size of MC being analyzed. An example of the results of region growing with tolerance $\tau = 0.025$ is shown as yellow within a radiologist defined ROI (outlined in red) in Fig. 3.1.

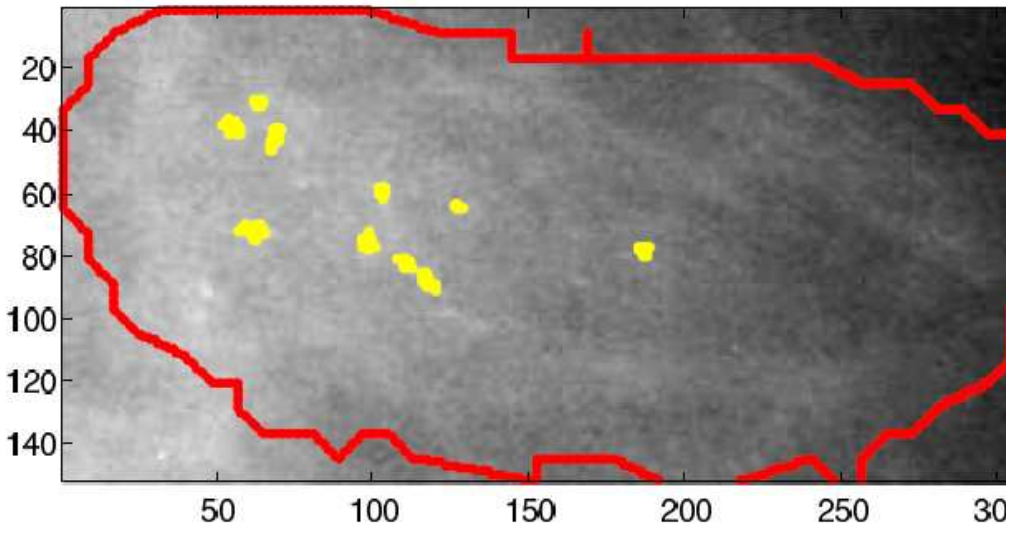


Figure 3.1: An example of the RGM. The yellow pixels are the result of the region growing segmentation.

## 3.2 Gradient Vector Flow Active Contour

The gradient vector flow (GVF) active contour, or snake [19] is used to get an order set of close contour points from the region growing results. Active contours are widely used in computer vision and image processing applications. Particularly it is used to outline boundaries of an object or other desired features within an image [20]. The snakes are curves defined within an image domain, which could move according to the internal force and the external gradient field until finally reaching a balanced state. Since the external gradient field is computed from the image data, the snake will conform to the boundaries of the object or other desired image feature. An example of active contour is provided in Fig. 3.2 [19]. The dynamic snake equation is defined in equation (3.2):

$$X(s,t) = \alpha X''(s,t) - \beta X'(s,t) + V(x,y) \tag{3.2}$$

where $\mathbf{X}(s,t) = [x(s,t), y(s,t)]$ is the snake and $s \in [0,1]$, $\mathbf{X}'$ and $\mathbf{X}''$ denote the first and second derivatives of $\mathbf{X}$ with respect to $s$, $\alpha$ and $\beta$ are weighting parameters applied to

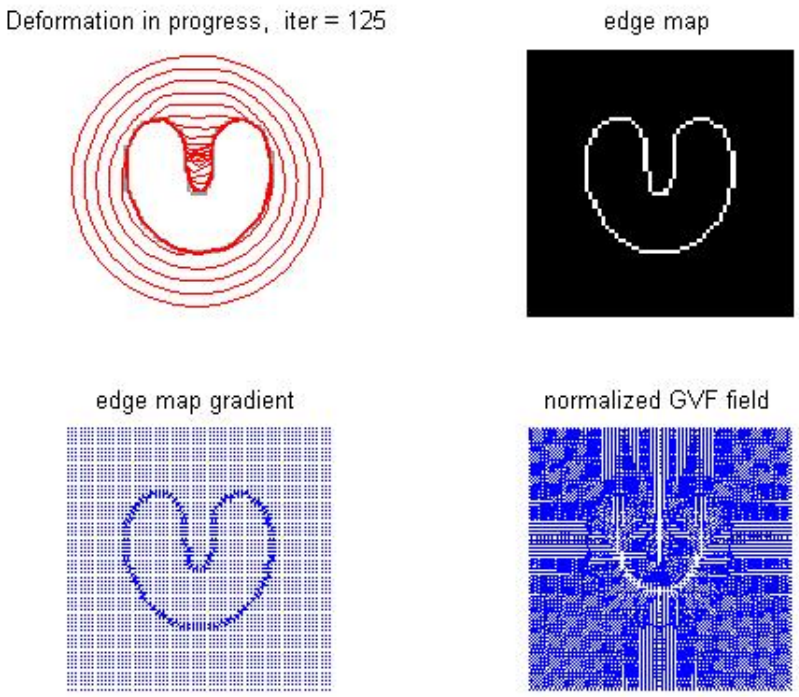


Figure 3.2: An example of active coutour

the snakes tension and rigidity, respectively. The last term of equation (3.2) is $V(x,y) = [u(x,y), v(x,y)]$, the gradient vector field that minimized the energy functional ε, defined in equation (3.3)

$$\varepsilon = \int\int \mu(u_x^2 + u_y^2 + v_x^2 + v_y^2) + |\nabla f|^2 |V(x,y) - \nabla f|^2 dxdy \tag{3.3}$$

where $f(x,y)$ is the edge map and $\mu$ is a parameter governing the tradeoff between the first term and the second term in the integrand.

## 3.3 A Normalized Distance Signature

The signature of a shape is used extensively in image processing shape analysis applications. The shape signature can be generated in various ways [21]. In [18], an order set

of close contour points of each MC within a radiologist defined ROI is required to extract shape features. A normalized distance signature is extracted from the order set of close contour from GVF contour described in the previous section of this chapter. The distance signature is defined as the Euclidean distance of the ordered contour point to the centroid [18] in equation (3.4)

$$\text{dist}[i] = \sqrt{(x_i - x_c)^2 + (y_i - y_c)^2}. \tag{3.4}$$

It should be noted that this distance signature is invariant to various affine transformations like translations and rotations. The distance signature of equation (3.4) will change with the size of an object. The scale variance is partly due to the digitizing error of the coordinate of the contour point, which in most of the cases has a negligible effect. Another reason why this signature is only pseudo-scale invariance is that a length of the normalized signature in equation (3.5) varies with respect to the size of the object and sampling of the contour. To make it pseudo-invariant to scale, the distance signature is normalized by dividing the mean. The normalized distance signature used in the proposed feature is

$$\widetilde{\text{dist}}[i] = \frac{\text{dist}[i]}{\text{mean}\,(\mathbf{dist})}\ . \tag{3.5}$$

This normalization provides a pseudo-scale invariance to the distance signature.

## 3.4 A Novel Roughness Metric

The novel aspect of the proposed method is using frequency analysis of the normalized distance signature to evaluate the roughness of a MC contour. Bandpass filtering is provided by a three level wavelet decomposition and reconstruction with a Daubechies eight tap wavelet. The reconstruction using only the third detail wavelet coefficients $\mathbf{D}_3$ is used to compute the roughness feature. In Fig. 3.3, the filtering processes is illustrated by a

block diagram. The filters $F_a(z)$, $G_a(z)$, $F_s(z)$, and $G_s(z)$ denote the $z$-transforms of the eight tap Daubechies analysis scaling function, analysis wavelet, synthesis scaling function, and synthesis wavelet, respectively. The processes denoted by $\downarrow 2$ and $\uparrow 2$ indicate down sampling and up sampling by a factor of two, respectively.

An example using a circle, an ellipse and a star shaped contour is displayed in Fig. 3.4.

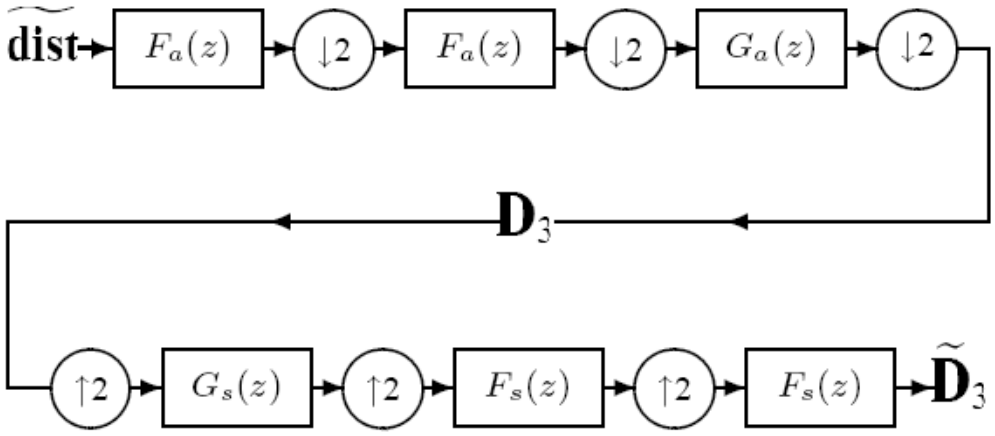


Figure 3.3: Wavelet decomposition of the normalized distance signature $\widetilde{\mathbf{dist}}$ and reconstruction from only the $\mathbf{D}_3$ coefficients.

The normalized distance signatures of circle, ellipse and star are shown in Fig. 3.5 as the green, blue, and red plots, respectively. The performance of the proposed metric is demonstrated by analyzing these three shapes. The filtering result of the normalized distance signatures is shown in Fig. 3.6.

Low frequency oscillations of the normalized distance signature indicate smoothness of the analyzed contour. It is shown by Fig. 3.5 that the normalized signature of the circle is constant and the star shaped contour has significantly higher frequency. To extract this higher frequency component of each normalized distance signature, reconstruction with only the $\widetilde{\mathbf{D}}_3$ coefficient of the normalized distance signature is employed. Fig. 3.6 shows the $\widetilde{\mathbf{D}}_3$ coefficient reconstruction of the circle, ellipse and star as the green, blue,

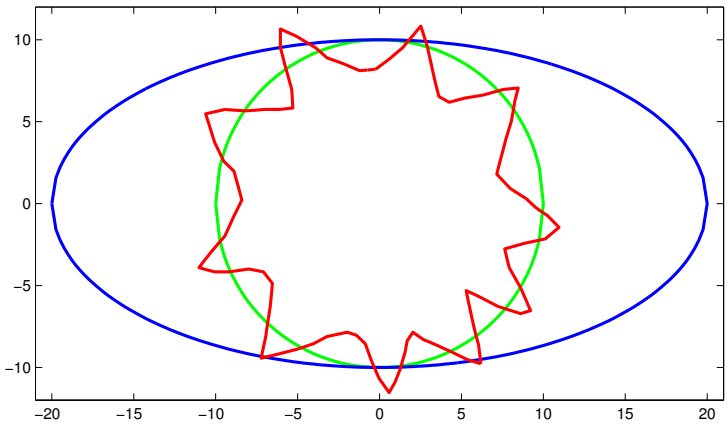


Figure 3.4: Example of an ellipse, a circle, and a star contours.

and red plots, respectively. A larger maximum absolute value of the $\widetilde{\mathbf{D}}_3$ reconstruction in Fig. 3.6 indicates a rougher contour. Therefore, the proposed novel metric $\alpha$ to classify MC is the maximum absolute value of reconstruction from the $\mathbf{D}_3$ coefficients

$$\alpha = \max(|\widetilde{\mathbf{D}}_3|). \tag{3.6}$$

The reason why absolute value is used as the shape feature is that a value in the reconstruction of $\widetilde{\mathbf{D}}_3$ would indicate a local difference. Whether this local difference will cause a positive or negative peak in the reconstruction of $\widetilde{\mathbf{D}}_3$ is dependent on how the filters are implemented. Also, a larger amplitude of the peak in the reconstruction of $\widetilde{\mathbf{D}}_3$ is attained by larger local differences. Further the absolute value makes the metric invariant to reflecting the contour about some line. A list of the roughness value $\alpha$ defined in equation (3.6) for the circle, ellipse, and the star shaped contour, as well as analysis using previously proposed shape feature is provided in Table 3.1. From Table 3.1, the roughness metric $\alpha$ has a desired relation that is substantially larger for the rough star shaped (0.1528) contour than for the circle (0) and the ellipse (0.0095).

A flow chart of my shape analysis method is shown in Fig. 3.7.

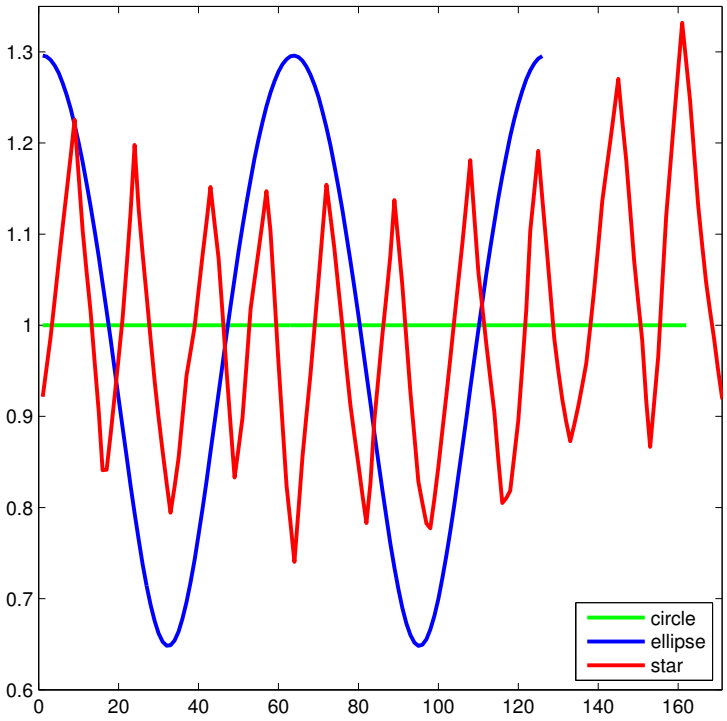


Figure 3.5: The normalized distance signatures ($\widetilde{\mathbf{dist}}$).

Table 3.1: Previously published and proposed α features of the contours shown in Fig. 3.4

| Contour | Moments | Fourier descriptor | Compactness | α |
|---|---|---|---|---|
| circle | 0 | 0.1166 | 12.5571 | 0 |
| ellipse | 0.0377 | 0.1215 | 14.9301 | 0.0095 |
| star | 0.0297 | 0.0587 | 29.136 | 0.1528 |

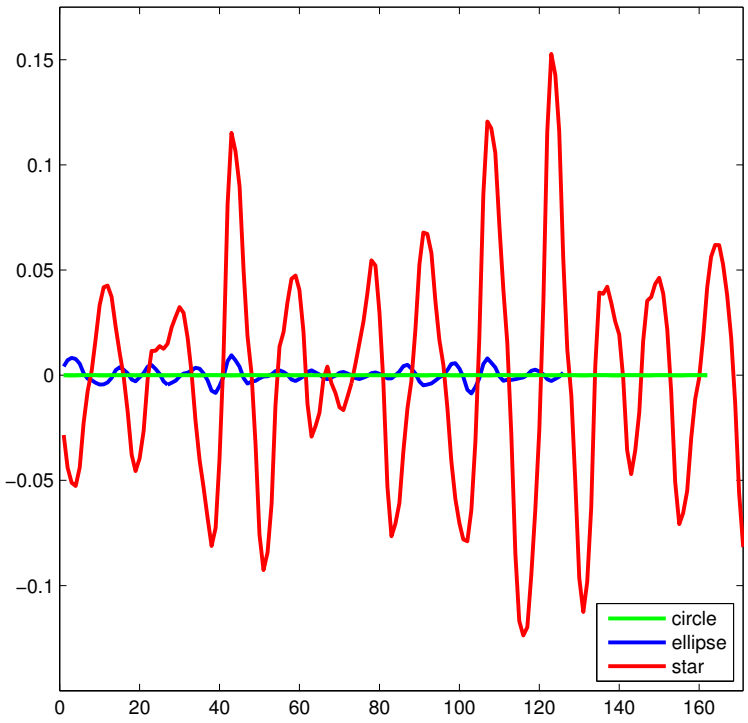


Figure 3.6: Approximations of the normalized distance signatures in Fig. 3.5 from using only the $\mathbf{D}_3$ wavelet coefficients.

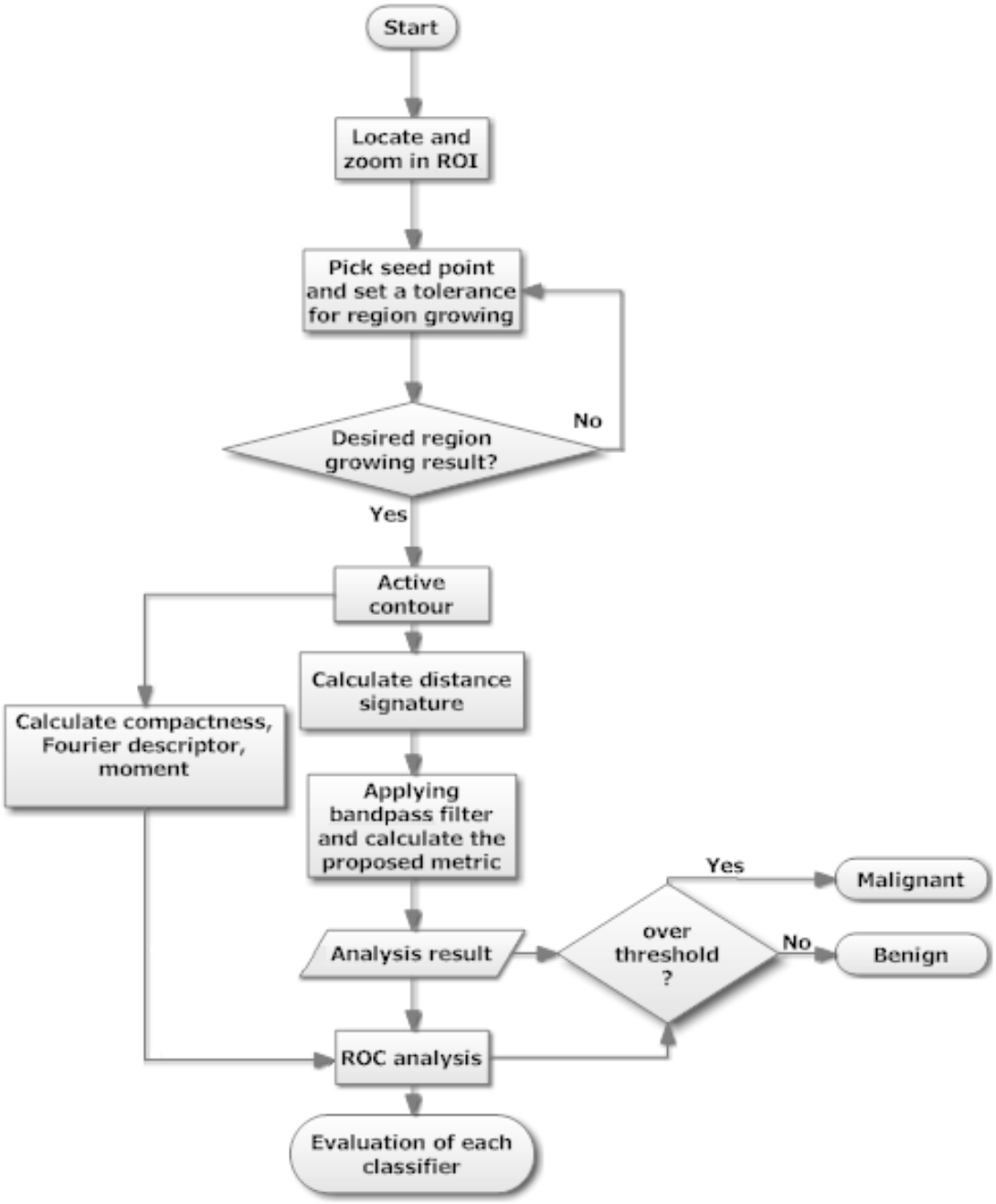


Figure 3.7: Flowchart of the proposed method

# CHAPTER 4: EXPERIMENTATION AND RESULT

An experiment was performed to evaluate the robustness of my proposed roughness metric. The experiment tested my proposed metric against three previously published shape metrics.

## 4.1 The Experimentation

A data mining of DDSM shows that mammograms with certain characteristics are problematic to diagnosis. The number of each lesion type in DDSM and the ratios of benign cases in each lesion type are listed in Table 4.1 and Table 4.2, respectively. In Table 4.2,

Table 4.1: Numbers of each lesion types in DDSM

| Type\Distribution | Cluster | Linear | Segmental | Regional | Diffuse |
|---|---|---|---|---|---|
| Punctate | 82 | 4 | 20 | 6 | 4 |
| Amorphous | 135 | 6 | 33 | 11 | 4 |
| Pleomorphic | 716 | 70 | 140 | 27 | 0 |
| Round & regular | 8 | 0 | 0 | 0 | 0 |
| Luscent center | 0 | 1 | 0 | 0 | 0 |
| Fine 2 branching | 28 | 36 | 19 | 2 | 0 |

the ratio of benign to total number of pleomorphic and cluster MC cases is close to 0.5. This indicates that it is difficult to classify mammograms with this type of lesion. An example of a DDSM case of pleomorphic and clustered mammogram with associate data file is included in Appendix A. Other cases that also have ratio of benign cases close to 0.5

Table 4.2: Ratios of benign cases

| Type\Distribution | Cluster | Linear | Segmental | Regional | Diffuse |
|---|---|---|---|---|---|
| Punctate | 0.65 | 1.0 | 0.8 | 0.6 | 1.0 |
| Amorphous | 0.79 | 0.3 | 0.79 | 0.45 | 0.5 |
| Pleomorphic | 0.59 | 0.17 | 0.3 | 0.2 | N/A |
| Round & regular | 0.75 | N/A | N/A | N/A | N/A |
| Luscent center | N/A | 1.0 | N/A | N/A | N/A |
| Fine 2 branching | 0.18 | 0.25 | 0 | 1.0 | N/A |

are ignored due to the small number of total cases.

The experiment was performed using 183 DDSM pleomorphic and clustered MC cases, from DDSM. This set included 58 malignant and 125 benign cases. There were a total of 368 individual MC that were analyzed. All 183 cases had only one radiologist defined ROI associated with each mammogram. The sole ROI contained BIRADS® pleomorphic and clustered MC and biopsy was recommended in all cases. Only MC from the ROI were analyzed. The robustness of the segmentation of each MC was supervised by setting the tolerance parameter by trial and error so that a robust segmentation was attained. The GVF algorithms was also supervised to ensure that the contour of each MC was correctly captured. The initial curve of GVF was a small circle centered at the centroid of the MC determined by the region growing algorithm. In [5], a radiologist prescribe that a cluster can be classified as benign when all MC within the ROI are round or oval. Thus, a single rough shaped MC could indicate the development of malignant cancer. Therefore the maximum $\alpha$ attained by a selected MC in a ROI is used to classify the ROI as benign or malignant. The shape features of compactness, moment and Fourier descriptor, as described in [18] are used as a comparison to test improvements provided by my shape feature.

## 4.2 Receiver Operating Characteristic

The receiver operating characteristic (ROC) graph is a technique to visualize the sensitivity and specificity of the performance of a certain classifier. It has been used in signal detection theory to describe the relation of hit rate and false alarm rate [22]. ROC is widely used to evaluate medical decision algorithms. The true positive rate (TPR), also called hit rate, represent the probability that a system could correctly classify given it is actually positive. The false positive rate (FPR), also called false alarm rate, indicates how often the system classify an actual negative as a positive. True positive rate (TPR) and false positive rate

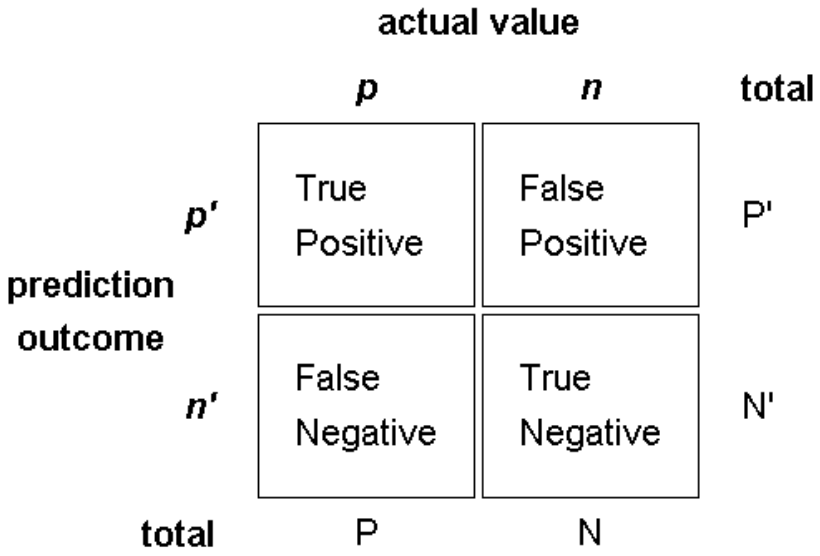


Figure 4.1: Relations between TPR, FPR, FNR and TNR

(FPR) are defined in equation (4.1) and equation (4.2) respectively, where TP is number of true positives, FN is number of false negatives, FP is number of false positives and TN is true negatives. The TPR and FPR are mathematically defined as

$$TPR = \frac{TP}{TP + FN} \tag{4.1}$$

$$FPR = \frac{FP}{FP+TN}. \tag{4.2}$$

To show the significance of the ROC, let's assume benign MC have a shape feature, whose values have a Gaussian distribution with $\mu = 1$ and $\sigma^2 = 0.49$, while the same feature of malignant MC have a Gaussian distribution with $\mu = -1$ and $\sigma^2 = 0.49$ as shown in the left plot of Fig. 4.2. If we choose 0.5 as the threshold of this classifier to determine the pathology, the TPR would be represented by the shaded part in the center plot of Fig. 4.2 while the FPR is represented by the shaded part in the right plot of Fig. 4.2. Though we

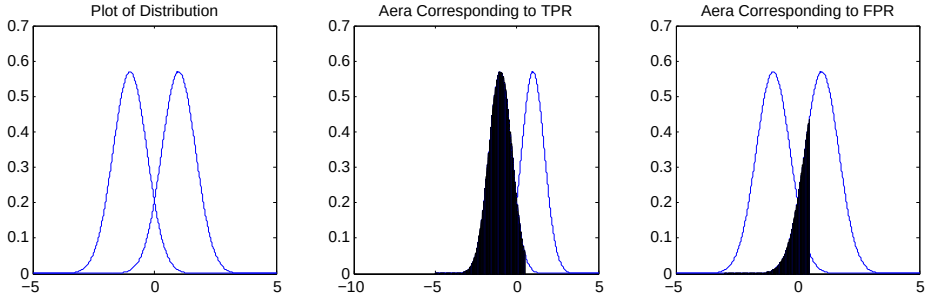


Figure 4.2: An example of distributions to illustrate TPR and FPR. These distribution are not actual.

could choose a different threshold to achieve a desired TPR or FPR, performance of the classifier is dependent on the overlap of the distributions. The ROC graph displays the dependence of the threshold on FPR and TPR. FPR is indicated on the x-axis and TPR is indicated on the y-axis. Fig. 4.3 shows an example of a ROC curve. It is widely quantified that a classifier with higher AUC (area under curve) is considered a better one, because it could achieve a higher TPR than one with lower AUC at the same FNR. The ROC curve and AUC are used to judge the performance of a classifier. It's ideal to get a 100% TPR with a 0% FPR. But in reality there is a trade off between these two. A simulated ROC curve is plotted in Fig. 4.3, if the threshold corresponding to the circle point on the ROC in Fig. 4.3 is used, we could achieve 35% FNR and 55% TPR performance.

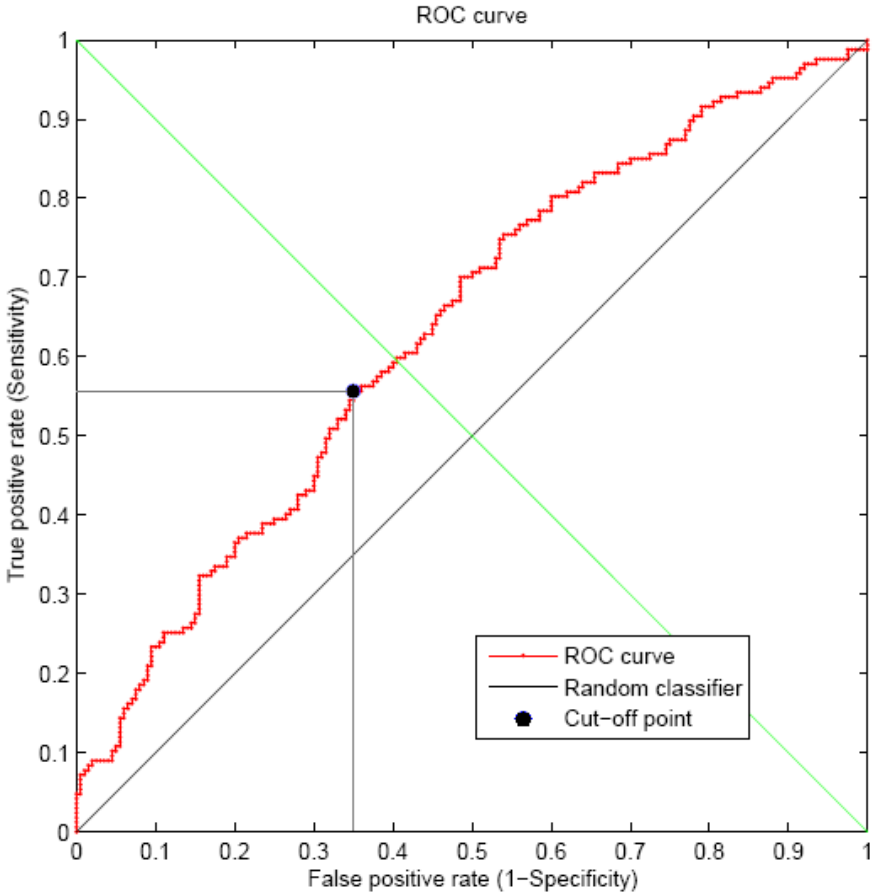


Figure 4.3: A simulated ROC curve

Table 4.3: AUC in Fig. 4.4

| Feature | AUC % |
|---|---|
| Proposed $\alpha$ | 96.4 |
| Moment | 78.0 |
| Fourier descriptor | 73.9 |
| Compactness | 56.5 |

## 4.3 Test Result

The shape feature of each of the 368 MCs was computed using my proposed method to produce an $\alpha$ value, along with the Fourier descriptor, moment and the compactness shape feature. These computed shape feature measures are listed in Table C.1. Only the maximum $\alpha$ from each ROI was used to classify the pathology. Appendix B lists the computed shape feature measures for the MC which has the maximum value in each ROI. The F, FF and C data in Appendix B were used to generate the ROC and calculate the AUC for those features. The ROC of the proposed a measure, along with the ROCs of the moment, Fourier, and compactness measures are shown in Fig. 4.4. The corresponding AUC of each these four ROCs are listed Table 4.3. The ROC of my proposed shape measure shows better diagnostic accuracy than the compactness, moment and Fourier descriptor measures. The ROI of the $\alpha$ measure has a higher TPR at a cost of lower FPR as shown in Fig. 4.4. The AUC of my proposed metric is significantly higher than the other three.

Since missing a suspicious malignant case could be fatal, achieving a 100% TPR is the priority in setting the threshold for the classifier. With the threshold for the proposed method set at $\alpha = 02522$, all the malignant ROIs are correctly identified with a 20% FPR. Thus, it would have save 80% of the suspicious but benign cases from biopsy. Therefore 80% (100 out of 125) of the tested cases were correctly identified as benign, and all 58 tested malignant cases were correctly identified.

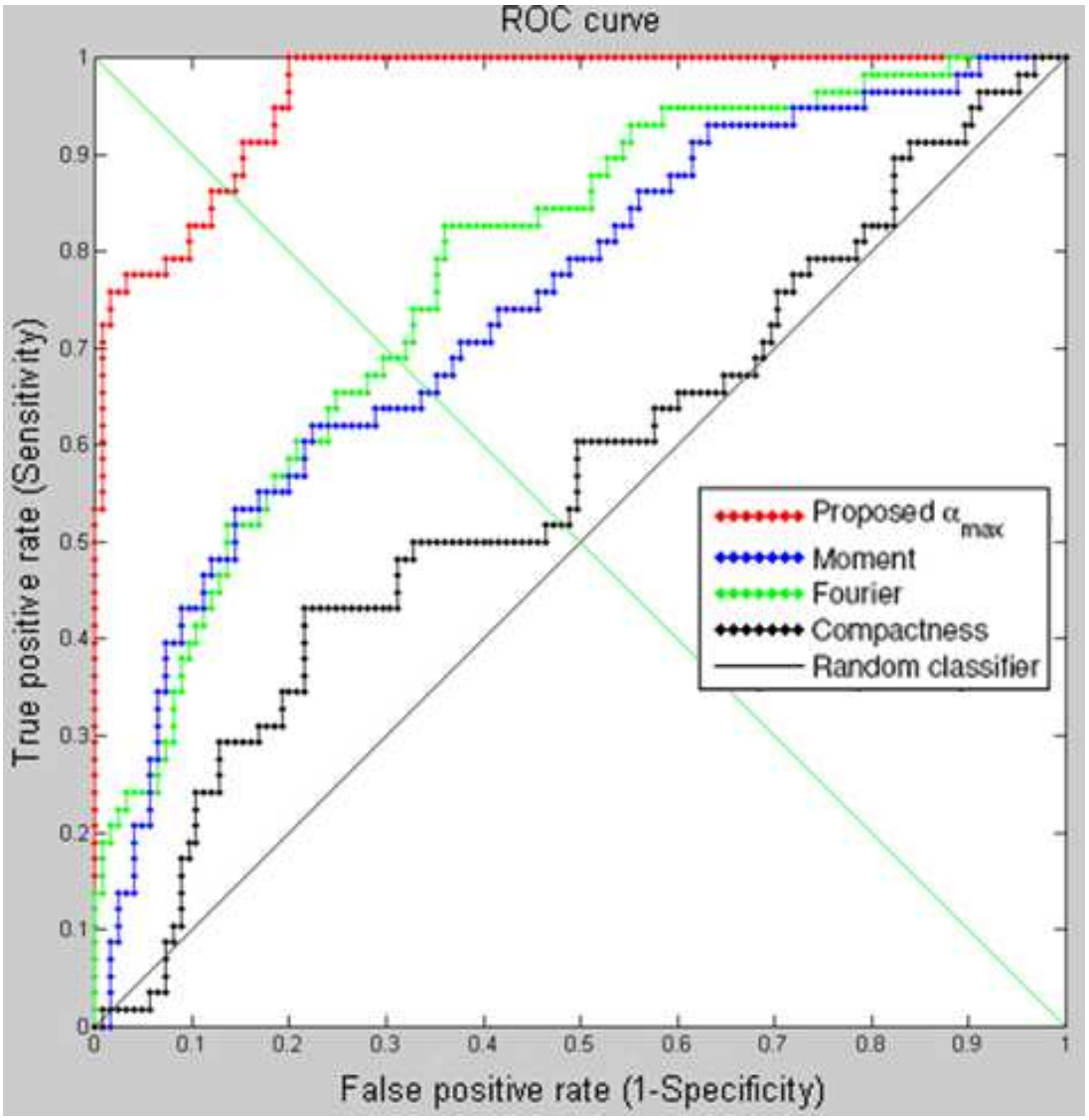


Figure 4.4: ROC of the proposed method, compactness, moment, Fourier descriptor

# CHAPTER 5: CONCLUSION

A computer aided method to assist radiologists in classifying mammograms with pleomorphic and clustered MC as well as other hard to diagnosis cases is presented in this thesis. As discussed in Chapter 1, it is standard to use mammography to detect early signs of breast cancer. Data mining of DDSM shows that ROIs with pleomorphic and clustered MC is problematic for radiologist to diagnose. Clinical evidence shows that ROIs containing tiny MC that are all round and oval have less of a chance in developing into malignant cancer [5]. Based on Sickles' claim in [5], an irregularly rough shaped MC could be an early sign of potentially malignant cancer.

The proposed method starts with a region growing process to segment the selected MC, followed by the generation of a GVF active contour to define the outer contour of ordered points of each segmented MC. Then a distance signature sequence is generated from the Euclidean distance of each contour points to the centroid. After normalizing the distance signature, a novel feature $\alpha$ to represent roughness of the shape is extracted by bandpass filtering and full resolution reconstruction of the normalized distance signature. A shape feature $\alpha$ is computed from the filtered sequence is produced by the maximum absolute value of the bandpass approximation of the normalized distance signature using only the $\mathbf{D}_3$ wavelet coefficients. High $\alpha$ values indicate rough shaped contours. An evaluation using ROC and AUC was performed. It was shown that the maximum $\alpha$ attain by a MC of each ROI was a better classifier of malignant or benign than the individual Fourier descriptor, moment and compactness features. Finally a threshold value for $\alpha$ is set by

ROC analysis to achieve 100% TPR at a low cost of 20% FPR. Therefore, the experimentation in this thesis provides evidence that my proposed shape analysis and metric is better classifier than any of the three previously published shape metrics.

# Appendices

# APPENDIX A: AN EXAMPLE OF THE DDSM DATA

Table A.1: An example of the DDSM data

| Pathology | Benign |
|---|---|
| Case No. | 1265 |
| Machine | HOWTEK |
| filename | A_1265_1.RIGHT_MLO |
| overlay file | A_1265_1.RIGHT_MLO.OVERLAY |

## A.1 Content of the associated ics file

ics_version 1.0

filename A-1265-1

DATE_OF_STUDY 25 1 1995

PATIENT_AGE 48

FILM

FILM_TYPE REGULAR

DENSITY 3

DATE_DIGITIZED 23 7 1998

DIGITIZER HOWTEK 43.5

SEQUENCE

LEFT_CC LINES 6556 PIXELS_PER_LINE 4111 BITS_PER_PIXEL 12 RESOLUTION

43.5 NON_OVERLAY

LEFT_MLO LINES 6616 PIXELS_PER_LINE 4081 BITS_PER_PIXEL 12 RESOLUTION 43.5 NON_OVERLAY

RIGHT_CC LINES 6646 PIXELS_PER_LINE 4066 BITS_PER_PIXEL 12 RESOLUTION 43.5 OVERLAY

RIGHT_MLO LINES 6871 PIXELS_PER_LINE 3961 BITS_PER_PIXEL 12 RESOLUTION 43.5 OVERLAY

## A.2 Content of overlay file

TOTAL_ABNORMALITIES 1

ABNORMALITY 1

LESION_TYPE CALCIFICATION TYPE PLEOMORPHIC DISTRIBUTION CLUSTERED

LESION_TYPE MASS SHAPE IRREGULAR MARGINS ILL_DEFINED

ASSESSMENT 4

SUBTLETY 3

PATHOLOGY BENIGN

TOTAL_OUTLINES 1

BOUNDARY

999 6165 0 0 0 0 0 6 6 6 6 6 6 6 6 6 6 6 6 6 0 0 0 0 0 6 6 6 6 6 7 7 7 7 7 6 6 6 6 6 0 0 0 0

6 6 6 6 0 0 0 0 0 6 6 6 6 6 0 0 0 0 0 6 6 6 6 6 0 0 0 0 0 6 6 6 6 6 7 7 7 7 7 6 6 6 6 6 0 0 0 0

0 6 6 6 6 6 6 6 6 6 0 0 0 0 6 6 6 6 6 6 6 6 6 0 0 0 0 0 6 6 6 6 6 6 6 6 6 6 7 7 7 7 0 6 6 6 6

6 0 0 0 0 0 6 6 6 6 6 0 0 0 0 0 6 6 6 6 6 0 0 0 0 0 6 6 6 6 6 0 0 0 0 7 7 7 7 7 0 0 0 0 0 0 0

0 0 0 0 0 0 0 0 0 0 0 0 2 2 2 2 2 0 0 0 0 0 0 0 0 0 2 2 2 2 2 0 0 0 0 0 1 1 1 1 1 2 2 2 2 2 1 1

1 1 1 2 2 2 2 2 2 2 2 2 2 2 2 2 2 2 0 0 0 0 0 2 2 2 2 2 2 2 2 2 2 2 2 2 2 2 2 2 2 2 0 0 0 0 2 2 2

2 2 2 2 2 2 2 2 2 2 2 2 2 2 2 2 2 2 2 2 2 2 2 2 2 2 2 2 2 2 2 2 2 2 2 2 2 2 2 2 2 2 2 2 2 2 2 2 2

2 2 4 4 4 4 2 2 2 2 2 3 3 3 3 3 2 2 2 2 2 4 4 4 4 4 2 2 2 2 2 2 2 2 2 2 4 4 4 4 4 2 2 2 2 2 2 2

2 2 3 3 3 3 3 2 2 2 2 2 4 4 4 4 4 2 2 2 2 2 2 2 2 2 2 2 4 4 4 4 4 3 3 3 3 4 2 2 2 2 2 4 4 4 4 4 2 2

2 2 2 4 4 4 4 4 4 4 4 4 4 4 2 2 2 2 2 4 4 4 4 4 4 4 4 4 4 4 4 4 4 4 4 4 4 4 4 4 4 4 5 5 5 5 5 4 4 4 4 4 4

4 4 4 4 6 6 6 6 6 4 4 4 4 4 4 4 4 4 4 6 6 6 6 6 4 4 4 4 4 6 6 6 6 6 5 5 5 5 5 6 6 6 6 6 4 4 4 4 4 6

6 6 6 6 4 4 4 4 4 6 6 6 6 6 4 4 4 4 4 6 6 6 6 6 4 4 4 4 4 6 6 6 6 6 6 6 6 6 6 4 4 4 4 4 6 6 6 6 6 6

6 6 6 6 5 5 5 5 5 #

## A.3 The image data

MC_BEN_1265 right medio-latheral raw pixel is displayed as a gray scale image in Fig. A.1. The circle in Fig A.1 is the ROI assigned by a radiologist.

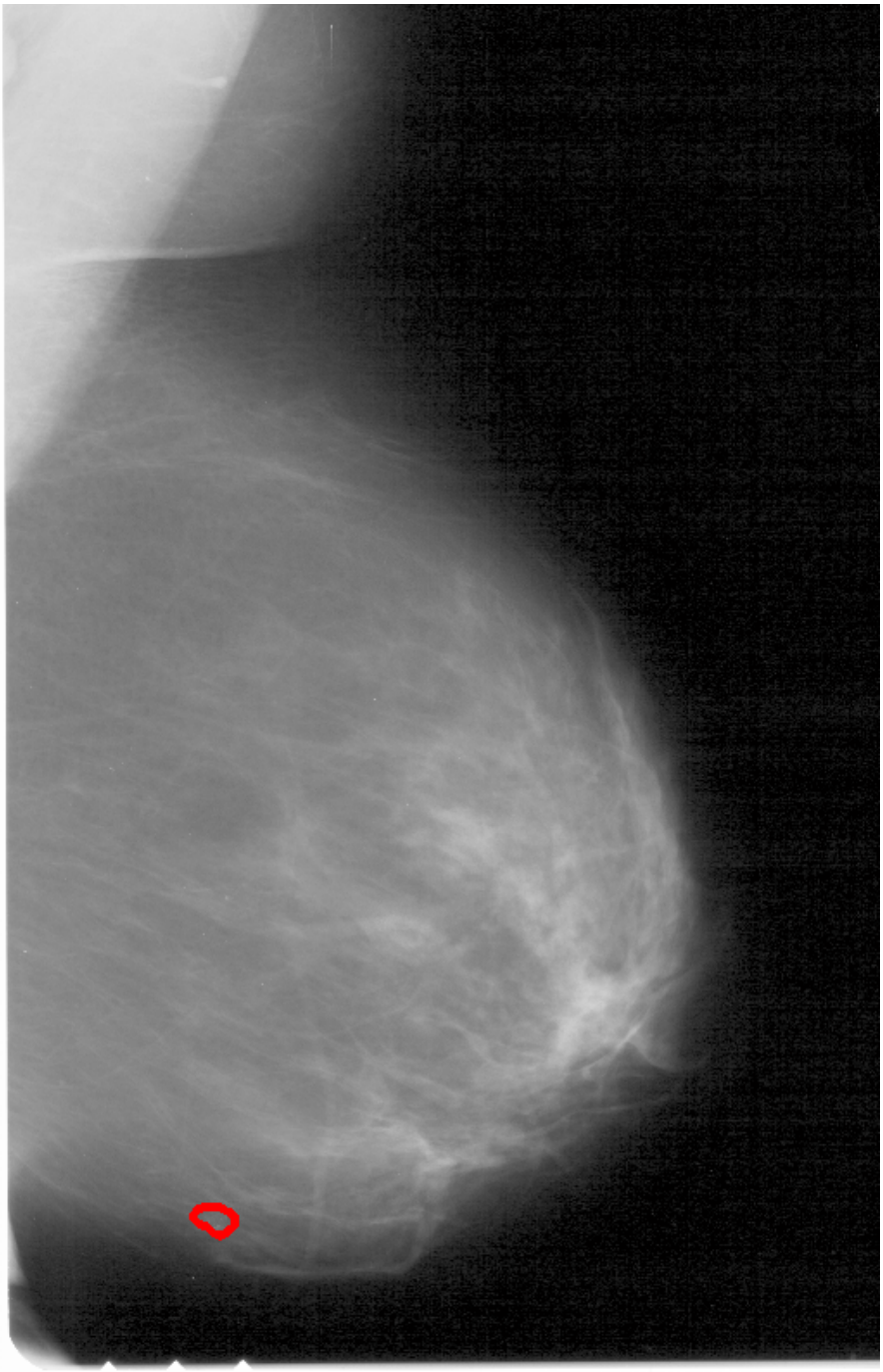

Figure A.1: An example of a DDSM data

# APPENDIX B: MICROCALCIFICATION WITH MAXIMUM α VALUE FOR EACH ROI

Table B.1: Microcalcification with maximum α value for each ROI

| DDSM case | α | Fourier | Moment | Compactness |
|---|---|---|---|---|
| MC_BEN_1259_1.mat | 0.084676431 | 0.025240216 | 0.614769548 | 10.77197715 |
| MC_BEN_1265_4.mat | 0.347223404 | 0.098615428 | 0.490803844 | 6.275492896 |
| MC_BEN_1272_2.mat | 0.19975872 | 0.04252498 | 0.582975705 | 8.810564978 |
| MC_BEN_1275_2.mat | 0.307238554 | 0.128832802 | 0.465227005 | 7.278547845 |
| MC_BEN_1280_2.mat | 0.175864578 | 0.022197345 | 0.598720818 | 9.71375325 |
| MC_BEN_1281_1.mat | 0.237342197 | 0.017690047 | 0.458650294 | 6.095371704 |
| MC_BEN_1285_1.mat | 0.309546224 | 0.037174297 | 0.446486919 | 7.098748289 |
| MC_BEN_1310_1.mat | 0.100753438 | 0.060198211 | 0.598568803 | 8.525565777 |
| MC_BEN_1315_2.mat | 0.266109429 | 0.093868379 | 0.506982529 | 8.664136631 |
| MC_BEN_1316_1.mat | 0.18662573 | 0.091708504 | 0.495537354 | 8.562449088 |
| MC_BEN_1324_1.mat | 0.12187249 | 0.044533998 | 0.542428748 | 12.15427163 |
| MC_BEN_1327_1.mat | 0.098433517 | 0.023290731 | 0.543439737 | 9.419546345 |
| MC_BEN_1328_3.mat | 0.113764708 | 0.041656053 | 0.529854072 | 9.393040294 |
| MC_BEN_1331_1.mat | 0.10741697 | 0.052157479 | 0.58483022 | 8.401850817 |
| MC_BEN_1333_1.mat | 0.120269727 | 0.033295635 | 0.545248786 | 7.796509185 |
| MC_BEN_1345_1.mat | 0.297595852 | 0.178357983 | 0.504386403 | 8.347717089 |
| MC_BEN_1352_2.mat | 0.284108936 | 0.029671215 | 0.53434663 | 10.41572376 |
| MC_BEN_1377_1.mat | 0.04417744 | 0.028339126 | 0.550486705 | 8.186040098 |
| MC_BEN_1378_1.mat | 0.122091168 | 0.044484385 | 0.535612658 | 8.299280465 |
| MC_BEN_1429_1.mat | 0.252155155 | 0.187341983 | 0.461769349 | 8.254601289 |
| MC_BEN_1438_1.mat | 0.084962262 | 0.01535973 | 0.604552061 | 9.9835409 |
| MC_BEN_1441_2.mat | 0.162174241 | 0.031139942 | 0.571004165 | 8.59893698 |
| MC_BEN_1448_5.mat | 0.127118954 | 0.029283897 | 0.61757009 | 10.39044896 |
| MC_BEN_1452_1.mat | 0.20984267 | 0.062868545 | 0.561836721 | 11.12415761 |
| MC_BEN_1458_2.mat | 0.31268102 | 0.054139773 | 0.52432661 | 11.65550049 |
| MC_BEN_1479_1.mat | 0.187935189 | 0.150003775 | 0.376170733 | 3.876132326 |
| MC_BEN_1497_1.mat | 0.1776908 | 0.067601149 | 0.546764185 | 8.030102703 |

Table B.1 – Continued

| DDSM case | α | Fourier | Moment | Compactness |
|---|---|---|---|---|
| MC_BEN_1513_2.mat | 0.13194451 | 0.038010922 | 0.602854259 | 10.62193633 |
| MC_BEN_1546_2.mat | 0.116896928 | 0.031586494 | 0.589910042 | 8.692571634 |
| MC_BEN_1551_2.mat | 0.145059977 | 0.142717991 | 0.483688246 | 6.536110046 |
| MC_BEN_1552_2.mat | 0.196022898 | 0.086496849 | 0.436794415 | 6.898970694 |
| MC_BEN_1561_1.mat | 0.222197223 | 0.099320461 | 0.478815596 | 11.37333273 |
| MC_BEN_1604_2.mat | 0.282848318 | 0.092711355 | 0.504224402 | 8.893919578 |
| MC_BEN_1632_1.mat | 0.123430676 | 0.019240017 | 0.573980409 | 6.840128839 |
| MC_BEN_1646_2.mat | 0.136648818 | 0.039310942 | 0.518871612 | 8.350427148 |
| MC_BEN_1648_2.mat | 0.299679548 | 0.042217244 | 0.527015096 | 8.617010368 |
| MC_BEN_1649_2.mat | 0.211849926 | 0.043997684 | 0.537139649 | 5.891021974 |
| MC_BEN_1655_2.mat | 0.176511778 | 0.048719788 | 0.539456337 | 8.295843086 |
| MC_BEN_1735_1.mat | 0.119490763 | 0.075223955 | 0.569468042 | 9.770666686 |
| MC_BEN_1736_2.mat | 0.227954306 | 0.165696322 | 0.408281499 | 3.487132 |
| MC_BEN_1740_1.mat | 0.12047272 | 0.028692231 | 0.443489736 | 3.383658912 |
| MC_BEN_1741_1.mat | 0.116360315 | 0.057894077 | 0.511477163 | 8.145009087 |
| MC_BEN_1743_4.mat | 0.109720627 | 0.027649728 | 0.65955228 | 10.3803839 |
| MC_BEN_1744_4.mat | 0.298760412 | 0.160611279 | 0.554986468 | 8.404989483 |
| MC_BEN_1746_2.mat | 0.135882476 | 0.117086102 | 0.520447882 | 10.92652108 |
| MC_BEN_1749_1.mat | 0.251275217 | 0.096698395 | 0.536471361 | 10.77884226 |
| MC_BEN_1751_1.mat | 0.137642946 | 0.019064038 | 0.571256551 | 6.41187649 |
| MC_BEN_1753_1.mat | 0.161871278 | 0.029903771 | 0.544078403 | 7.185790994 |
| MC_BEN_1755_1.mat | 0.269785189 | 0.053789531 | 0.506523931 | 3.725730725 |
| MC_BEN_1760_1.mat | 0.157180432 | 0.031581169 | 0.535636749 | 11.72943651 |
| MC_BEN_1762_3.mat | 0.141313026 | 0.019141173 | 0.526837071 | 9.476811879 |
| MC_BEN_1774_1.mat | 0.140113508 | 0.073104531 | 0.571719087 | 8.933101838 |
| MC_BEN_1775_2.mat | 0.129098043 | 0.052038356 | 0.529923929 | 10.23513392 |
| MC_BEN_1791_1.mat | 0.075548868 | 0.034063085 | 0.553693435 | 9.984340992 |
| MC_BEN_1806_1.mat | 0.162037178 | 0.067946998 | 0.55827106 | 11.17646723 |
| MC_BEN_1807_1.mat | 0.119032463 | 0.025040852 | 0.530869684 | 8.148352477 |
| MC_BEN_1818_1.mat | 0.074053438 | 0.028140046 | 0.579897789 | 11.0924612 |
| MC_BEN_1829_1.mat | 0.175414282 | 0.050085998 | 0.600359615 | 9.452233238 |
| MC_BEN_1839_3.mat | 0.19387208 | 0.056848963 | 0.568130992 | 8.851765591 |
| MC_BEN_1844_3.mat | 0.211831534 | 0.097614139 | 0.572290301 | 10.25076383 |
| MC_BEN_1854_2.mat | 0.275745524 | 0.107729608 | 0.426754439 | 5.731524928 |

Table B.1 – Continued

| DDSM case | α | Fourier | Moment | Compactness |
|---|---|---|---|---|
| MC_BEN_1859_1.mat | 0.097685122 | 0.029189451 | 0.557385169 | 9.253884991 |
| MC_BEN_1864_1.mat | 0.289145129 | 0.253900115 | 0.390073331 | 3.601533865 |
| MC_BEN_1866_3.mat | 0.239783652 | 0.075311783 | 0.491325395 | 13.67271548 |
| MC_BEN_1867_2.mat | 0.072810784 | 0.027126906 | 0.574181373 | 4.601949431 |
| MC_BEN_1868_4.mat | 0.212729421 | 0.083208875 | 0.565738659 | 10.08918177 |
| MC_BEN_1870_1.mat | 0.157951025 | 0.04381759 | 0.53032733 | 9.374086889 |
| MC_BEN_1883_2.mat | 0.174341254 | 0.064742059 | 0.521634264 | 8.842924457 |
| MC_BEN_1891_3.mat | 0.309329762 | 0.097452288 | 0.438930814 | 7.402733643 |
| MC_BEN_1909_1.mat | 0.18982443 | 0.05064472 | 0.587308283 | 10.15049265 |
| MC_BEN_1810_1.mat | 0.208772845 | 0.113735428 | 0.508240137 | 7.77000038 |
| MC_BEN_1913_1.mat | 0.153849094 | 0.050200854 | 0.539014765 | 6.854436674 |
| MC_BEN_1914_2.mat | 0.140756371 | 0.025582419 | 0.470753774 | 3.9861419 |
| MC_BEN_1919_1.mat | 0.207050568 | 0.094576784 | 0.525250717 | 6.322383379 |
| MC_BEN_1923_1.mat | 0.15648614 | 0.111472902 | 0.531782791 | 7.568149171 |
| MC_BEN_1924_1.mat | 0.26052208 | 0.077936745 | 0.535047193 | 9.706566101 |
| MC_BEN_1925_2.mat | 0.142916184 | 0.099369024 | 0.5057077 | 8.706285416 |
| MC_BEN_1926_2.mat | 0.230994626 | 0.099597288 | 0.508985208 | 4.903648901 |
| MC_BEN_1935_2.mat | 0.122161088 | 0.032322241 | 0.568010725 | 7.527438287 |
| MC_BEN_1944_2.mat | 0.074539088 | 0.021776604 | 0.581924399 | 4.700994026 |
| MC_BEN_1945_2.mat | 0.235715368 | 0.052547324 | 0.478283253 | 11.95492102 |
| MC_BEN_1949_1.mat | 0.18349787 | 0.133491298 | 0.489285859 | 8.177304507 |
| MC_BEN_1953_1.mat | 0.148433677 | 0.047074708 | 0.489683071 | 9.87323803 |
| MC_BEN_236_1.mat | 0.03611096 | 0.026877529 | 0.721452799 | 11.65276467 |
| MC_BEN_242_1.mat | 0.215991537 | 0.09482873 | 0.547788832 | 11.32481955 |
| MC_BEN_272_2.mat | 0.19285309 | 0.04664157 | 0.472461752 | 6.626807254 |
| MC_BEN_281_1.mat | 0.256007421 | 0.118713061 | 0.437578831 | 7.31377138 |
| MC_BEN_300_1.mat | 0.080088734 | 0.030952231 | 0.559494298 | 8.241624679 |
| MC_BEN_301_2.mat | 0.122658959 | 0.060489579 | 0.53672005 | 9.853453993 |
| MC_BEN_307_6.mat | 0.090573327 | 0.02651801 | 0.662553259 | 11.07401733 |
| MC_BEN_315_1.mat | 0.275655885 | 0.073929006 | 0.483081529 | 8.910022167 |
| MC_BEN_375_3.mat | 0.132834731 | 0.036762227 | 0.524491058 | 7.367340189 |
| MC_BEN_379_1.mat | 0.087574698 | 0.020663597 | 0.545480485 | 9.252053437 |
| MC_BEN_390_2.mat | 0.171372115 | 0.050093408 | 0.556085569 | 10.84750429 |
| MC_BEN_391_2.mat | 0.264145456 | 0.179927615 | 0.496953644 | 11.03708282 |

Table B.1 – Continued

| DDSM case | α | Fourier | Moment | Compactness |
|---|---|---|---|---|
| MC_BEN_400_1.mat | 0.223013595 | 0.0537195 | 0.460600319 | 7.854228687 |
| MC_BEN_409_1.mat | 0.250726678 | 0.090103446 | 0.459862987 | 8.575346769 |
| MC_BEN_412_2.mat | 0.163326876 | 0.11976707 | 0.476834382 | 6.459242578 |
| MC_BEN_466_1.mat | 0.191607247 | 0.044737435 | 0.464235692 | 8.972168663 |
| MC_BEN_476_2.mat | 0.208673277 | 0.057665175 | 0.573991942 | 8.893155447 |
| MC_BEN_486_1.mat | 0.115452647 | 0.06761639 | 0.487405951 | 7.12593918 |
| MC_BEN_486_1.mat | 0.225406225 | 0.049678189 | 0.499694181 | 12.11182743 |
| MC_BEN_492_1.mat | 0.240111809 | 0.024398173 | 0.471701072 | 7.961396342 |
| MC_BEN_500_1.mat | 0.26416649 | 0.089350269 | 0.469659468 | 12.45963728 |
| MC_BEN_502_2.mat | 0.094701262 | 0.054511274 | 0.529356454 | 8.994683334 |
| MC_BEN_508_2.mat | 0.192660008 | 0.071574437 | 0.402172903 | 3.0905081 |
| MC_BEN_3092_1.mat | 0.045326595 | 0.016826897 | 0.611459618 | 10.78233669 |
| MC_BEN_3094_3.mat | 0.096328372 | 0.039695173 | 0.566121067 | 10.99798263 |
| MC_BEN_3141_1.mat | 0.26446823 | 0.062446106 | 0.405635645 | 8.861520736 |
| MC_BEN_3145_1.mat | 0.156787559 | 0.014927636 | 0.473589469 | 5.972793304 |
| MC_BEN_3365_1.mat | 0.161553676 | 0.062121053 | 0.553952719 | 9.616617034 |
| MC_BEN_3367_1.mat | 0.198938596 | 0.138071224 | 0.466385739 | 8.235886941 |
| MC_BEN_3436_1.mat | 0.245282993 | 0.124279487 | 0.526764818 | 6.488217321 |
| MC_BEN_3437_1.mat | 0.154825102 | 0.031369339 | 0.506701622 | 8.043157306 |
| MC_BEN_3455_1.mat | 0.151923276 | 0.03377004 | 0.606752589 | 11.75606809 |
| MC_BEN_3456_2.mat | 0.191694169 | 0.083437569 | 0.416514298 | 4.204619055 |
| MC_BEN_3457_1.mat | 0.174002525 | 0.042168244 | 0.539639772 | 7.210099175 |
| MC_BEN_3459_1.mat | 0.146061643 | 0.021862321 | 0.596334268 | 10.06187453 |
| MC_BEN_3465_1.mat | 0.093699906 | 0.043648452 | 0.670753962 | 11.04484382 |
| MC_BEN_3470_1.mat | 0.161012804 | 0.089538139 | 0.482766005 | 12.46845749 |
| MC_BEN_3472_2.mat | 0.133992435 | 0.042718634 | 0.558000465 | 6.340218519 |
| MC_BEN_3473_1.mat | 0.184482442 | 0.041751233 | 0.563811172 | 9.530185699 |
| MC_BEN_3486_3.mat | 0.178689974 | 0.10954331 | 0.505537906 | 5.0265508 |
| MC_BEN_3493_1.mat | 0.248624834 | 0.027391573 | 0.504882192 | 7.591592118 |
| MC_BEN_3494_2.mat | 0.139721654 | 0.029152606 | 0.552592905 | 10.10404913 |
| MC_MAL_1133_2.mat | 0.528737747 | 0.377447031 | 0.36383988 | 4.845661779 |
| MC_MAL_1148_3.mat | 0.33041194 | 0.149666687 | 0.469996884 | 11.05426209 |
| MC_MAL_1152_4.mat | 0.172003283 | 0.052078644 | 0.426732332 | 7.994123988 |
| MC_MAL_1153_3.mat | 0.28414292 | 0.083882634 | 0.52621936 | 9.143124751 |

Table B.1 – Continued

| DDSM case | α | Fourier | Moment | Compactness |
|---|---|---|---|---|
| MC_MAL_1185_3.mat | 0.112192246 | 0.128492554 | 0.467475407 | 9.0448637 |
| MC_MAL_1188_3.mat | 0.291342338 | 0.055304239 | 0.560161147 | 12.09495169 |
| MC_MAL_1201_3.mat | 0.317095561 | 0.089999468 | 0.422986739 | 6.240750261 |
| MC_MAL_1212_2.mat | 0.256480673 | 0.056049615 | 0.561035336 | 10.79214147 |
| MC_MAL_1213_7.mat | 0.124627097 | 0.02417126 | 0.509627126 | 6.363471119 |
| MC_MAL_1214_6.mat | 0.079253238 | 0.032063042 | 0.592798761 | 9.791501017 |
| MC_MAL_1223_3.mat | 0.255613256 | 0.052903122 | 0.527444142 | 9.879499745 |
| MC_MAL_1235_3.mat | 0.39296243 | 0.094585245 | 0.532589484 | 11.65540818 |
| MC_MAL_1238_2.mat | 0.484097037 | 0.211800168 | 0.41440072 | 5.035175176 |
| MC_MAL_1245_2.mat | 0.43324245 | 0.15264398 | 0.538230696 | 9.121849255 |
| MC_MAL_1248_6.mat | 0.289252978 | 0.040623363 | 0.499020452 | 9.075978768 |
| MC_MAL_1250_4.mat | 0.37360809 | 0.075499953 | 0.49961605 | 8.730505406 |
| MC_MAL_1256_2.mat | 0.304906035 | 0.10100377 | 0.445495553 | 10.0780595 |
| MC_MAL_1257_3.mat | 0.234096514 | 0.04498372 | 0.548822149 | 6.562069065 |
| MC_MAL_1261_2.mat | 0.254609044 | 0.147282865 | 0.520753742 | 9.871731751 |
| MC_MAL_1489_3.mat | 0.263603928 | 0.056305188 | 0.497930208 | 8.601244908 |
| MC_MAL_1500_4.mat | 0.116269126 | 0.080335843 | 0.537378749 | 10.50014809 |
| MC_MAL_1528_3.mat | 0.18436958 | 0.070862081 | 0.402003621 | 4.324873083 |
| MC_MAL_1531_3.mat | 0.319234481 | 0.087314144 | 0.51174632 | 10.82943995 |
| MC_MAL_1585_2.mat | 0.383554559 | 0.106952859 | 0.459923552 | 6.969219653 |
| MC_MAL_1590_1.mat | 0.311934405 | 0.137503952 | 0.441563734 | 6.809559505 |
| MC_MAL_1596_3.mat | 0.184663726 | 0.047623899 | 0.486958923 | 7.068926005 |
| MC_MAL_1614_1.mat | 0.279711636 | 0.185862161 | 0.391656876 | 2.370364398 |
| MC_MAL_1637_3.mat | 0.343815373 | 0.34637897 | 0.42792009 | 5.172230163 |
| MC_MAL_1675_1.mat | 0.453423306 | 0.296936482 | 0.400399786 | 6.102914113 |
| MC_MAL_1819_6.mat | 0.049790479 | 0.024865456 | 0.608561588 | 9.123623387 |
| MC_MAL_1894_1.mat | 0.338617962 | 0.353741483 | 0.369843643 | 4.051984831 |
| MC_MAL_1897_5.mat | 0.293965363 | 0.102611262 | 0.557918215 | 9.152596853 |
| MC_MAL_1905_1.mat | 0.363717075 | 0.078664382 | 0.505186397 | 11.71062071 |
| MC_MAL_1907_2.mat | 0.084295431 | 0.021871202 | 0.57131448 | 6.179503044 |
| MC_MAL_4151_5.mat | 0.157774791 | 0.118388393 | 0.558258221 | 9.230696185 |
| MC_MAL_4117_2.mat | 0.252391081 | 0.027172212 | 0.427275323 | 4.72104505 |
| MC_MAL_4158_1.mat | 0.272765728 | 0.188414977 | 0.393244502 | 4.642228102 |
| MC_MAL_4161_2.mat | 0.298070732 | 0.06641729 | 0.470328725 | 6.944532205 |

Table B.1 – Continued

| DDSM case | α | Fourier | Moment | Compactness |
|---|---|---|---|---|
| MC_MAL_4182_5.mat | 0.217062366 | 0.030990162 | 0.568507446 | 11.1376256 |
| MC_MAL_63_4.mat | 0.05078913 | 0.039441553 | 0.645653922 | 9.650091481 |
| MC_MAL_87_2.mat | 0.199702352 | 0.067467241 | 0.563289444 | 8.563738456 |
| MC_MAL_90_2.mat | 0.265606749 | 0.098405971 | 0.539460706 | 9.889550053 |
| MC_MAL_96_2.mat | 0.234687875 | 0.074800255 | 0.470739498 | 7.629193722 |
| MC_MAL_99_2.mat | 0.188015136 | 0.137714018 | 0.455260326 | 9.278270858 |
| MC_MAL_106_4.mat | 0.139996976 | 0.044309131 | 0.561431326 | 8.777875486 |
| MC_MAL_132_3.mat | 0.286655134 | 0.053970416 | 0.465514088 | 8.720718134 |
| MC_MAL_167_1.mat | 0.388661871 | 0.456851315 | 0.352259982 | 5.694313149 |
| MC_MAL_171_3.mat | 0.225700483 | 0.077972193 | 0.547883075 | 8.712827494 |
| MC_MAL_309_3.mat | 0.388581978 | 0.05315112 | 0.439518347 | 8.969793882 |
| MC_MAL_3044_4.mat | 0.141011138 | 0.025996265 | 0.556078786 | 7.753603423 |
| MC_MAL_3055_5.mat | 0.199965258 | 0.052269033 | 0.479480094 | 9.188225493 |
| MC_MAL_3382_3.mat | 0.328638051 | 0.122335785 | 0.591837158 | 10.63397466 |
| MC_MAL_3389_2.mat | 0.109308743 | 0.042350634 | 0.626327556 | 9.9927393 |
| MC_MAL_3406_2.mat | 0.357365892 | 0.084558158 | 0.436413 | 9.28687106 |
| MC_MAL_3476_5.mat | 0.346551973 | 0.097383541 | 0.430315119 | 5.791465025 |
| MC_MAL_3498_2.mat | 0.290699714 | 0.091543027 | 0.41481946 | 10.65937887 |
| MC_MAL_3504_2.mat | 0.472145662 | 0.162701336 | 0.504748288 | 9.841025799 |
| MC_MAL_3512_5.mat | 0.089739537 | 0.01109452 | 0.632236507 | 10.01128331 |

# APPENDIX C: TEST RESULT OF ALL MICROCALCIFICATIONS

Table C.1: Test result of all Microcalcifications

| DDSM case | α | Fourier | Moment | Compactness |
|---|---|---|---|---|
| MC_BEN_1259_1.mat | 0.084676431 | 0.025240216 | 0.614769548 | 10.77197715 |
| MC_BEN_1265_4.mat | 0.347223404 | 0.098615428 | 0.490803844 | 6.275492896 |
| MC_BEN_1265_4.mat | 0.297898778 | 0.060605516 | 0.457782693 | 6.577760302 |
| MC_BEN_1265_4.mat | 0.216795795 | 0.042637401 | 0.501735552 | 7.127286181 |
| MC_BEN_1265_4.mat | 0.183348459 | 0.020060262 | 0.548460946 | 6.591384054 |
| MC_BEN_1272_2.mat | 0.19975872 | 0.04252498 | 0.582975705 | 8.810564978 |
| MC_BEN_1272_2.mat | 0.168662412 | 0.086794622 | 0.560598761 | 9.943083386 |
| MC_BEN_1275_2.mat | 0.307238554 | 0.128832802 | 0.465227005 | 7.278547845 |
| MC_BEN_1275_2.mat | 0.223423099 | 0.031963097 | 0.56807436 | 11.63147179 |
| MC_BEN_1280_2.mat | 0.175864578 | 0.022197345 | 0.598720818 | 9.71375325 |
| MC_BEN_1280_2.mat | 0.158236324 | 0.077995207 | 0.584773321 | 8.9832727 |
| MC_BEN_1281_1.mat | 0.237342197 | 0.017690047 | 0.458650294 | 6.095371704 |
| MC_BEN_1285_1.mat | 0.309546224 | 0.037174297 | 0.446486919 | 7.098748289 |
| MC_BEN_1310_1.mat | 0.100753438 | 0.060198211 | 0.598568803 | 8.525565777 |
| MC_BEN_1315_2.mat | 0.266109429 | 0.093868379 | 0.506982529 | 8.664136631 |
| MC_BEN_1315_2.mat | 0.287394278 | 0.042281446 | 0.513034326 | 10.44401844 |
| MC_BEN_1316_1.mat | 0.18662573 | 0.091708504 | 0.495537354 | 8.562449088 |
| MC_BEN_1324_1.mat | 0.12187249 | 0.044533998 | 0.542428748 | 12.15427163 |
| MC_BEN_1327_1.mat | 0.098433517 | 0.023290731 | 0.543439737 | 9.419546345 |
| MC_BEN_1328_3.mat | 0.113764708 | 0.041656053 | 0.529854072 | 9.393040294 |
| MC_BEN_1328_3.mat | 0.241670388 | 0.162111536 | 0.387854206 | 4.274333802 |
| MC_BEN_1328_3.mat | 0.157785358 | 0.098004272 | 0.533503079 | 9.022604575 |
| MC_BEN_1331_1.mat | 0.10741697 | 0.052157479 | 0.58483022 | 8.401850817 |
| MC_BEN_1333_1.mat | 0.120269727 | 0.033295635 | 0.545248786 | 7.796509185 |
| MC_BEN_1345_1.mat | 0.297595852 | 0.178357983 | 0.504386403 | 8.347717089 |
| MC_BEN_1352_2.mat | 0.284108936 | 0.029671215 | 0.53434663 | 10.41572376 |
| MC_BEN_1352_2.mat | 0.073400738 | 0.02294978 | 0.492543078 | 7.732298033 |
| MC_BEN_1377_1.mat | 0.04417744 | 0.028339126 | 0.550486705 | 8.186040098 |
| MC_BEN_1378_1.mat | 0.122091168 | 0.044484385 | 0.535612658 | 8.299280465 |

Table C.1 – Continued

| DDSM case | α | Fourier | Moment | Compactness |
|---|---|---|---|---|
| MC_BEN_1429_1.mat | 0.252155155 | 0.187341983 | 0.461769349 | 8.254601289 |
| MC_BEN_1438_1.mat | 0.084962262 | 0.01535973 | 0.604552061 | 9.9835409 |
| MC_BEN_1441_2.mat | 0.162174241 | 0.031139942 | 0.571004165 | 8.59893698 |
| MC_BEN_1441_2.mat | 0.279243597 | 0.105341045 | 0.561645049 | 10.16309533 |
| MC_BEN_1448_5.mat | 0.127118954 | 0.029283897 | 0.61757009 | 10.39044896 |
| MC_BEN_1448_5.mat | 0.184722411 | 0.075796868 | 0.566136959 | 10.22171802 |
| MC_BEN_1448_5.mat | 0.154813213 | 0.054406874 | 0.502941041 | 7.959480803 |
| MC_BEN_1448_5.mat | 0.155887688 | 0.053570233 | 0.532988734 | 8.104517765 |
| MC_BEN_1448_5.mat | 0.295652852 | 0.090213412 | 0.517314076 | 7.58913176 |
| MC_BEN_1452_1.mat | 0.20984267 | 0.062868545 | 0.561836721 | 11.12415761 |
| MC_BEN_1458_2.mat | 0.31268102 | 0.054139773 | 0.52432661 | 11.65550049 |
| MC_BEN_1458_2.mat | 0.281954769 | 0.036392862 | 0.531580527 | 7.187885731 |
| MC_BEN_1479_1.mat | 0.187935189 | 0.150003775 | 0.376170733 | 3.876132326 |
| MC_BEN_1497_1.mat | 0.1776908 | 0.067601149 | 0.546764185 | 8.030102703 |
| MC_BEN_1513_2.mat | 0.13194451 | 0.038010922 | 0.602854259 | 10.62193633 |
| MC_BEN_1513_2.mat | 0.214365471 | 0.051067462 | 0.502229212 | 9.184008586 |
| MC_BEN_1546_2.mat | 0.116896928 | 0.031586494 | 0.589910042 | 8.692571634 |
| MC_BEN_1546_2.mat | 0.156773191 | 0.020678976 | 0.483978334 | 8.245882606 |
| MC_BEN_1551_2.mat | 0.145059977 | 0.142717991 | 0.483688246 | 6.536110046 |
| MC_BEN_1551_2.mat | 0.127551018 | 0.037996084 | 0.541450043 | 8.377847325 |
| MC_BEN_1552_2.mat | 0.196022898 | 0.086496849 | 0.436794415 | 6.898970694 |
| MC_BEN_1552_2.mat | 0.154094774 | 0.103507531 | 0.559176306 | 11.46409708 |
| MC_BEN_1561_1.mat | 0.222197223 | 0.099320461 | 0.478815596 | 11.37333273 |
| MC_BEN_1604_2.mat | 0.282848318 | 0.092711355 | 0.504224402 | 8.893919578 |
| MC_BEN_1604_2.mat | 0.207058997 | 0.113735076 | 0.487965194 | 7.747930085 |
| MC_BEN_1632_1.mat | 0.123430676 | 0.019240017 | 0.573980409 | 6.840128839 |
| MC_BEN_1646_2.mat | 0.136648818 | 0.039310942 | 0.518871612 | 8.350427148 |
| MC_BEN_1646_2.mat | 0.15907701 | 0.147039305 | 0.447876167 | 8.832799424 |
| MC_BEN_1648_2.mat | 0.299679548 | 0.042217244 | 0.527015096 | 8.617010368 |
| MC_BEN_1648_2.mat | 0.149953568 | 0.025059129 | 0.585679818 | 7.75484615 |
| MC_BEN_1649_2.mat | 0.211849926 | 0.043997684 | 0.537139649 | 5.891021974 |
| MC_BEN_1649_2.mat | 0.158438223 | 0.069128332 | 0.596577673 | 10.96006251 |
| MC_BEN_1655_2.mat | 0.176511778 | 0.048719788 | 0.539456337 | 8.295843086 |
| MC_BEN_1655_2.mat | 0.239845366 | 0.062024079 | 0.567465572 | 13.89001336 |

Table C.1 – Continued

| DDSM case | α | Fourier | Moment | Compactness |
|---|---|---|---|---|
| MC_BEN_1735_1.mat | 0.119490763 | 0.075223955 | 0.569468042 | 9.770666686 |
| MC_BEN_1736_2.mat | 0.227954306 | 0.165696322 | 0.408281499 | 3.487132 |
| MC_BEN_1736_2.mat | 0.139333386 | 0.043179018 | 0.495722497 | 6.009852343 |
| MC_BEN_1740_1.mat | 0.12047272 | 0.028692231 | 0.443489736 | 3.383658912 |
| MC_BEN_1741_1.mat | 0.116360315 | 0.057894077 | 0.511477163 | 8.145009087 |
| MC_BEN_1743_4.mat | 0.109720627 | 0.027649728 | 0.65955228 | 10.3803839 |
| MC_BEN_1743_4.mat | 0.154046789 | 0.022801152 | 0.534727501 | 9.537066388 |
| MC_BEN_1743_4.mat | 0.203673971 | 0.088027606 | 0.557680593 | 8.470288397 |
| MC_BEN_1743_4.mat | 0.183206395 | 0.039589007 | 0.520898341 | 9.062050715 |
| MC_BEN_1744_4.mat | 0.298760412 | 0.160611279 | 0.554986468 | 8.404989483 |
| MC_BEN_1744_4.mat | 0.140875512 | 0.044835472 | 0.559811991 | 8.591445988 |
| MC_BEN_1744_4.mat | 0.092481359 | 0.039419603 | 0.537756321 | 9.975493922 |
| MC_BEN_1744_4.mat | 0.19306068 | 0.092038621 | 0.560352356 | 8.777179664 |
| MC_BEN_1746_2.mat | 0.135882476 | 0.117086102 | 0.520447882 | 10.92652108 |
| MC_BEN_1746_2.mat | 0.164118188 | 0.053338082 | 0.607605035 | 9.350094563 |
| MC_BEN_1749_1.mat | 0.251275217 | 0.096698395 | 0.536471361 | 10.77884226 |
| MC_BEN_1751_1.mat | 0.137642946 | 0.019064038 | 0.571256551 | 6.41187649 |
| MC_BEN_1753_1.mat | 0.161871278 | 0.029903771 | 0.544078403 | 7.185790994 |
| MC_BEN_1755_1.mat | 0.269785189 | 0.053789531 | 0.506523931 | 3.725730725 |
| MC_BEN_1760_1.mat | 0.157180432 | 0.031581169 | 0.535636749 | 11.72943651 |
| MC_BEN_1762_3.mat | 0.141313026 | 0.019141173 | 0.526837071 | 9.476811879 |
| MC_BEN_1762_3.mat | 0.10822825 | 0.024993541 | 0.612515246 | 11.43339485 |
| MC_BEN_1762_3.mat | 0.161754961 | 0.067125346 | 0.478995082 | 8.766313533 |
| MC_BEN_1774_1.mat | 0.140113508 | 0.073104531 | 0.571719087 | 8.933101838 |
| MC_BEN_1775_2.mat | 0.129098043 | 0.052038356 | 0.529923929 | 10.23513392 |
| MC_BEN_1775_2.mat | 0.289002343 | 0.05973641 | 0.466124454 | 14.38419187 |
| MC_BEN_1791_1.mat | 0.075548868 | 0.034063085 | 0.553693435 | 9.984340992 |
| MC_BEN_1806_1.mat | 0.162037178 | 0.067946998 | 0.55827106 | 11.17646723 |
| MC_BEN_1807_1.mat | 0.119032463 | 0.025040852 | 0.530869684 | 8.148352477 |
| MC_BEN_1818_1.mat | 0.074053438 | 0.028140046 | 0.579897789 | 11.0924612 |
| MC_BEN_1829_1.mat | 0.175414282 | 0.050085998 | 0.600359615 | 9.452233238 |
| MC_BEN_1839_3.mat | 0.19387208 | 0.056848963 | 0.568130992 | 8.851765591 |
| MC_BEN_1839_3.mat | 0.140775917 | 0.025612741 | 0.628046522 | 8.220338289 |
| MC_BEN_1839_3.mat | 0.116204302 | 0.01703115 | 0.542380604 | 9.365111881 |

Table C.1 – Continued

| DDSM case | α | Fourier | Moment | Compactness |
|---|---|---|---|---|
| MC_BEN_1844_3.mat | 0.211831534 | 0.097614139 | 0.572290301 | 10.25076383 |
| MC_BEN_1844_3.mat | 0.139177116 | 0.132136454 | 0.462039811 | 6.545781014 |
| MC_BEN_1844_3.mat | 0.150970189 | 0.080242697 | 0.52561792 | 12.70921559 |
| MC_BEN_1854_2.mat | 0.275745524 | 0.107729608 | 0.426754439 | 5.731524928 |
| MC_BEN_1854_2.mat | 0.246715265 | 0.053511034 | 0.504672361 | 12.95686846 |
| MC_BEN_1859_1.mat | 0.097685122 | 0.029189451 | 0.557385169 | 9.253884991 |
| MC_BEN_1864_1.mat | 0.289145129 | 0.253900115 | 0.390073331 | 3.601533865 |
| MC_BEN_1866_3.mat | 0.239783652 | 0.075311783 | 0.491325395 | 13.67271548 |
| MC_BEN_1866_3.mat | 0.127563966 | 0.034854475 | 0.525734293 | 7.824421309 |
| MC_BEN_1866_3.mat | 0.163882378 | 0.168122627 | 0.516214383 | 11.68083524 |
| MC_BEN_1867_2.mat | 0.072810784 | 0.027126906 | 0.574181373 | 4.601949431 |
| MC_BEN_1867_2.mat | 0.158980857 | 0.065722699 | 0.539673904 | 12.30758983 |
| MC_BEN_1868_4.mat | 0.212729421 | 0.083208875 | 0.565738659 | 10.08918177 |
| MC_BEN_1868_4.mat | 0.103591522 | 0.031013346 | 0.582783838 | 8.520153259 |
| MC_BEN_1868_4.mat | 0.167698655 | 0.064594591 | 0.509318149 | 9.392178771 |
| MC_BEN_1868_4.mat | 0.23394732 | 0.07084572 | 0.539334529 | 12.83632261 |
| MC_BEN_1870_1.mat | 0.157951025 | 0.04381759 | 0.53032733 | 9.374086889 |
| MC_BEN_1883_2.mat | 0.174341254 | 0.064742059 | 0.521634264 | 8.842924457 |
| MC_BEN_1883_2.mat | 0.168211836 | 0.060707107 | 0.553070718 | 6.912239378 |
| MC_BEN_1891_3.mat | 0.309329762 | 0.097452288 | 0.438930814 | 7.402733643 |
| MC_BEN_1891_3.mat | 0.280132051 | 0.089097766 | 0.463254453 | 6.63288486 |
| MC_BEN_1891_3.mat | 0.200447058 | 0.090514992 | 0.394159668 | 3.273168413 |
| MC_BEN_1909_1.mat | 0.18982443 | 0.05064472 | 0.587308283 | 10.15049265 |
| MC_BEN_1810_1.mat | 0.208772845 | 0.113735428 | 0.508240137 | 7.77000038 |
| MC_BEN_1913_1.mat | 0.153849094 | 0.050200854 | 0.539014765 | 6.854436674 |
| MC_BEN_1914_2.mat | 0.140756371 | 0.025582419 | 0.470753774 | 3.9861419 |
| MC_BEN_1914_2.mat | 0.207431444 | 0.082145525 | 0.54420566 | 4.820228797 |
| MC_BEN_1919_1.mat | 0.207050568 | 0.094576784 | 0.525250717 | 6.322383379 |
| MC_BEN_1923_1.mat | 0.15648614 | 0.111472902 | 0.531782791 | 7.568149171 |
| MC_BEN_1924_1.mat | 0.26052208 | 0.077936745 | 0.535047193 | 9.706566101 |
| MC_BEN_1925_2.mat | 0.142916184 | 0.099369024 | 0.5057077 | 8.706285416 |
| MC_BEN_1925_2.mat | 0.226849494 | 0.092693502 | 0.327806206 | 1.704884918 |
| MC_BEN_1926_2.mat | 0.230994626 | 0.099597288 | 0.508985208 | 4.903648901 |
| MC_BEN_1926_2.mat | 0.137058478 | 0.038402301 | 0.555504532 | 4.884648204 |

Table C.1 – Continued

| DDSM case | α | Fourier | Moment | Compactness |
|---|---|---|---|---|
| MC_BEN_1935_2.mat | 0.122161088 | 0.032322241 | 0.568010725 | 7.527438287 |
| MC_BEN_1935_2.mat | 0.176768781 | 0.05336069 | 0.523683099 | 10.05813958 |
| MC_BEN_1944_2.mat | 0.074539088 | 0.021776604 | 0.581924399 | 4.700994026 |
| MC_BEN_1944_2.mat | 0.225042001 | 0.028798321 | 0.561924346 | 6.657550062 |
| MC_BEN_1945_2.mat | 0.235715368 | 0.052547324 | 0.478283253 | 11.95492102 |
| MC_BEN_1945_2.mat | 0.25563091 | 0.063607192 | 0.433109195 | 7.273062918 |
| MC_BEN_1949_1.mat | 0.18349787 | 0.133491298 | 0.489285859 | 8.177304507 |
| MC_BEN_1953_1.mat | 0.148433677 | 0.047074708 | 0.489683071 | 9.87323803 |
| MC_BEN_236_1.mat | 0.03611096 | 0.026877529 | 0.721452799 | 11.65276467 |
| MC_BEN_242_1.mat | 0.215991537 | 0.09482873 | 0.547788832 | 11.32481955 |
| MC_BEN_272_2.mat | 0.19285309 | 0.04664157 | 0.472461752 | 6.626807254 |
| MC_BEN_272_2.mat | 0.133565826 | 0.058062166 | 0.415959654 | 4.980920643 |
| MC_BEN_281_1.mat | 0.256007421 | 0.118713061 | 0.437578831 | 7.31377138 |
| MC_BEN_300_1.mat | 0.080088734 | 0.030952231 | 0.559494298 | 8.241624679 |
| MC_BEN_301_2.mat | 0.122658959 | 0.060489579 | 0.53672005 | 9.853453993 |
| MC_BEN_301_2.mat | 0.122658959 | 0.060489579 | 0.53672005 | 9.853453993 |
| MC_BEN_307_6.mat | 0.090573327 | 0.02651801 | 0.662553259 | 11.07401733 |
| MC_BEN_307_6.mat | 0.091385275 | 0.036510017 | 0.588151702 | 11.20120709 |
| MC_BEN_307_6.mat | 0.122065266 | 0.065240284 | 0.554541442 | 10.35081242 |
| MC_BEN_307_6.mat | 0.184919261 | 0.039458613 | 0.5415229 | 9.699468874 |
| MC_BEN_315_1.mat | 0.275655885 | 0.073929006 | 0.483081529 | 8.910022167 |
| MC_BEN_375_3.mat | 0.132834731 | 0.036762227 | 0.524491058 | 7.367340189 |
| MC_BEN_375_3.mat | 0.218686562 | 0.063129618 | 0.523975958 | 10.63535362 |
| MC_BEN_375_3.mat | 0.197721243 | 0.048412198 | 0.557123438 | 10.76963788 |
| MC_BEN_379_1.mat | 0.087574698 | 0.020663597 | 0.545480485 | 9.252053437 |
| MC_BEN_390_2.mat | 0.171372115 | 0.050093408 | 0.556085569 | 10.84750429 |
| MC_BEN_390_2.mat | 0.190459437 | 0.040789942 | 0.551022548 | 9.453572471 |
| MC_BEN_391_2.mat | 0.264145456 | 0.179927615 | 0.496953644 | 11.03708282 |
| MC_BEN_391_2.mat | 0.186536385 | 0.046829194 | 0.543529582 | 10.43013586 |
| MC_BEN_400_1.mat | 0.223013595 | 0.0537195 | 0.460600319 | 7.854228687 |
| MC_BEN_409_1.mat | 0.250726678 | 0.090103446 | 0.459862987 | 8.575346769 |
| MC_BEN_412_2.mat | 0.163326876 | 0.11976707 | 0.476834382 | 6.459242578 |
| MC_BEN_412_2.mat | 0.200445295 | 0.073989382 | 0.459862296 | 10.12313383 |
| MC_BEN_466_1.mat | 0.191607247 | 0.044737435 | 0.464235692 | 8.972168663 |

Table C.1 – Continued

| DDSM case | α | Fourier | Moment | Compactness |
|---|---|---|---|---|
| MC_BEN_476_2.mat | 0.208673277 | 0.057665175 | 0.573991942 | 8.893155447 |
| MC_BEN_476_2.mat | 0.24646867 | 0.096153315 | 0.472533011 | 5.220144046 |
| MC_BEN_486_1.mat | 0.115452647 | 0.06761639 | 0.487405951 | 7.12593918 |
| MC_BEN_486_1.mat | 0.225406225 | 0.049678189 | 0.499694181 | 12.11182743 |
| MC_BEN_492_1.mat | 0.240111809 | 0.024398173 | 0.471701072 | 7.961396342 |
| MC_BEN_500_1.mat | 0.26416649 | 0.089350269 | 0.469659468 | 12.45963728 |
| MC_BEN_502_2.mat | 0.094701262 | 0.054511274 | 0.529356454 | 8.994683334 |
| MC_BEN_502_2.mat | 0.21031948 | 0.083684518 | 0.521463639 | 11.10729399 |
| MC_BEN_508_2.mat | 0.192660008 | 0.071574437 | 0.402172903 | 3.0905081 |
| MC_BEN_508_2.mat | 0.248606286 | 0.191414641 | 0.344394973 | 3.798421303 |
| MC_BEN_3092_1.mat | 0.045326595 | 0.016826897 | 0.611459618 | 10.78233669 |
| MC_BEN_3094_3.mat | 0.096328372 | 0.039695173 | 0.566121067 | 10.99798263 |
| MC_BEN_3094_3.mat | 0.13701773 | 0.059576101 | 0.511834644 | 9.420967303 |
| MC_BEN_3094_3.mat | 0.227977324 | 0.172388719 | 0.432564591 | 6.727420425 |
| MC_BEN_3141_1.mat | 0.26446823 | 0.062446106 | 0.405635645 | 8.861520736 |
| MC_BEN_3145_1.mat | 0.156787559 | 0.014927636 | 0.473589469 | 5.972793304 |
| MC_BEN_3365_1.mat | 0.161553676 | 0.062121053 | 0.553952719 | 9.616617034 |
| MC_BEN_3367_1.mat | 0.198938596 | 0.138071224 | 0.466385739 | 8.235886941 |
| MC_BEN_3436_1.mat | 0.245282993 | 0.124279487 | 0.526764818 | 6.488217321 |
| MC_BEN_3437_1.mat | 0.154825102 | 0.031369339 | 0.506701622 | 8.043157306 |
| MC_BEN_3455_1.mat | 0.151923276 | 0.03377004 | 0.606752589 | 11.75606809 |
| MC_BEN_3456_2.mat | 0.191694169 | 0.083437569 | 0.416514298 | 4.204619055 |
| MC_BEN_3457_1.mat | 0.174002525 | 0.042168244 | 0.539639772 | 7.210099175 |
| MC_BEN_3459_1.mat | 0.146061643 | 0.021862321 | 0.596334268 | 10.06187453 |
| MC_BEN_3465_1.mat | 0.093699906 | 0.043648452 | 0.670753962 | 11.04484382 |
| MC_BEN_3470_1.mat | 0.161012804 | 0.089538139 | 0.482766005 | 12.46845749 |
| MC_BEN_3472_2.mat | 0.133992435 | 0.042718634 | 0.558000465 | 6.340218519 |
| MC_BEN_3472_2.mat | 0.233406192 | 0.192973426 | 0.447272752 | 7.373999743 |
| MC_BEN_3473_1.mat | 0.184482442 | 0.041751233 | 0.563811172 | 9.530185699 |
| MC_BEN_3486_3.mat | 0.178689974 | 0.10954331 | 0.505537906 | 5.0265508 |
| MC_BEN_3486_3.mat | 0.154567397 | 0.108149977 | 0.542109841 | 11.04708078 |
| MC_BEN_3486_3.mat | 0.283103556 | 0.110944304 | 0.501304952 | 12.15268346 |
| MC_BEN_3493_1.mat | 0.248624834 | 0.027391573 | 0.504882192 | 7.591592118 |
| MC_BEN_3494_2.mat | 0.139721654 | 0.029152606 | 0.552592905 | 10.10404913 |

Table C.1 – Continued

| DDSM case | α | Fourier | Moment | Compactness |
|---|---|---|---|---|
| MC_BEN_3494_2.mat | 0.155505113 | 0.034026408 | 0.492395738 | 10.66144207 |
| MC_MAL_1133_2.mat | 0.528737747 | 0.377447031 | 0.36383988 | 4.845661779 |
| MC_MAL_1133_2.mat | 0.345500653 | 0.088929271 | 0.439578153 | 12.94972812 |
| MC_MAL_1148_3.mat | 0.33041194 | 0.149666687 | 0.469996884 | 11.05426209 |
| MC_MAL_1148_3.mat | 0.282804711 | 0.151408563 | 0.481554818 | 8.532901089 |
| MC_MAL_1148_3.mat | 0.181621259 | 0.064488477 | 0.508974985 | 6.956158918 |
| MC_MAL_1152_4.mat | 0.172003283 | 0.052078644 | 0.426732332 | 7.994123988 |
| MC_MAL_1152_4.mat | 0.216414992 | 0.10098766 | 0.432927446 | 7.077399794 |
| MC_MAL_1152_4.mat | 0.455556123 | 0.078908976 | 0.430316652 | 7.60142201 |
| MC_MAL_1152_4.mat | 0.222613356 | 0.023175378 | 0.564635592 | 7.180828656 |
| MC_MAL_1153_3.mat | 0.28414292 | 0.083882634 | 0.52621936 | 9.143124751 |
| MC_MAL_1153_3.mat | 0.148640108 | 0.056693612 | 0.477384507 | 6.936419176 |
| MC_MAL_1185_3.mat | 0.112192246 | 0.128492554 | 0.467475407 | 9.0448637 |
| MC_MAL_1185_3.mat | 0.191160486 | 0.11644072 | 0.5612425 | 9.041645597 |
| MC_MAL_1185_3.mat | 0.422788998 | 0.060199006 | 0.536082378 | 9.744836693 |
| MC_MAL_1188_3.mat | 0.291342338 | 0.055304239 | 0.560161147 | 12.09495169 |
| MC_MAL_1188_3.mat | 0.355078026 | 0.191564467 | 0.522751453 | 10.92719035 |
| MC_MAL_1188_3.mat | 0.319565169 | 0.063210004 | 0.570607285 | 10.94244664 |
| MC_MAL_1201_3.mat | 0.317095561 | 0.089999468 | 0.422986739 | 6.240750261 |
| MC_MAL_1201_3.mat | 0.237329422 | 0.103454395 | 0.428335636 | 7.023826361 |
| MC_MAL_1201_3.mat | 0.12478339 | 0.05777666 | 0.539548369 | 6.745810699 |
| MC_MAL_1212_2.mat | 0.256480673 | 0.056049615 | 0.561035336 | 10.79214147 |
| MC_MAL_1212_2.mat | 0.207005331 | 0.056406896 | 0.493295602 | 11.56877473 |
| MC_MAL_1213_7.mat | 0.124627097 | 0.02417126 | 0.509627126 | 6.363471119 |
| MC_MAL_1213_7.mat | 0.17518174 | 0.074580629 | 0.52457311 | 9.317780736 |
| MC_MAL_1213_7.mat | 0.451484839 | 0.140444439 | 0.469012625 | 7.66219232 |
| MC_MAL_1213_7.mat | 0.209321493 | 0.0501448 | 0.425808854 | 8.441036208 |
| MC_MAL_1213_7.mat | 0.284478239 | 0.076442209 | 0.472535592 | 8.233720437 |
| MC_MAL_1213_7.mat | 0.268503243 | 0.053629271 | 0.450112581 | 6.541356035 |
| MC_MAL_1213_7.mat | 0.375283767 | 0.10293157 | 0.372789888 | 2.975391114 |
| MC_MAL_1214_6.mat | 0.079253238 | 0.032063042 | 0.592798761 | 9.791501017 |
| MC_MAL_1214_6.mat | 0.39059576 | 0.143260547 | 0.44571901 | 7.0591608 |
| MC_MAL_1214_6.mat | 0.339051086 | 0.09554589 | 0.497510121 | 10.09102722 |
| MC_MAL_1214_6.mat | 0.103350291 | 0.03460591 | 0.591183777 | 9.394354864 |

Table C.1 – Continued

| DDSM case | α | Fourier | Moment | Compactness |
|---|---|---|---|---|
| MC_MAL_1214_6.mat | 0.19930135 | 0.078774046 | 0.519117524 | 8.414158555 |
| MC_MAL_1214_6.mat | 0.36603128 | 0.127318583 | 0.40003035 | 4.061326333 |
| MC_MAL_1223_3.mat | 0.255613256 | 0.052903122 | 0.527444142 | 9.879499745 |
| MC_MAL_1223_3.mat | 0.235853133 | 0.248806213 | 0.403156396 | 4.919354882 |
| MC_MAL_1235_3.mat | 0.39296243 | 0.094585245 | 0.532589484 | 11.65540818 |
| MC_MAL_1235_3.mat | 0.208009425 | 0.079584351 | 0.571023519 | 9.824522933 |
| MC_MAL_1238_2.mat | 0.484097037 | 0.211800168 | 0.41440072 | 5.035175176 |
| MC_MAL_1238_2.mat | 0.20074468 | 0.029757436 | 0.464596509 | 8.449023035 |
| MC_MAL_1245_2.mat | 0.43324245 | 0.15264398 | 0.538230696 | 9.121849255 |
| MC_MAL_1245_2.mat | 0.28321241 | 0.042379796 | 0.440460067 | 7.581632299 |
| MC_MAL_1248_6.mat | 0.289252978 | 0.040623363 | 0.499020452 | 9.075978768 |
| MC_MAL_1248_6.mat | 0.269235083 | 0.091200075 | 0.490501948 | 7.75839403 |
| MC_MAL_1248_6.mat | 0.080673041 | 0.043435079 | 0.513082354 | 8.336028628 |
| MC_MAL_1248_6.mat | 0.19290129 | 0.031510256 | 0.555956459 | 10.3854849 |
| MC_MAL_1248_6.mat | 0.086438382 | 0.059918017 | 0.540071163 | 8.506924567 |
| MC_MAL_1248_6.mat | 0.361972944 | 0.119994061 | 0.537285735 | 10.86065139 |
| MC_MAL_1250_4.mat | 0.37360809 | 0.075499953 | 0.49961605 | 8.730505406 |
| MC_MAL_1250_4.mat | 0.165665193 | 0.031474468 | 0.550206476 | 6.496065785 |
| MC_MAL_1250_4.mat | 0.253827278 | 0.101299899 | 0.461560265 | 7.112848874 |
| MC_MAL_1250_4.mat | 0.207104177 | 0.077034705 | 0.495977236 | 6.776767741 |
| MC_MAL_1256_2.mat | 0.304906035 | 0.10100377 | 0.445495553 | 10.0780595 |
| MC_MAL_1256_2.mat | 0.414237226 | 0.10275239 | 0.4166295 | 4.390579975 |
| MC_MAL_1257_3.mat | 0.234096514 | 0.04498372 | 0.548822149 | 6.562069065 |
| MC_MAL_1257_3.mat | 0.528834096 | 0.279729819 | 0.44030754 | 6.955589185 |
| MC_MAL_1261_2.mat | 0.254609044 | 0.147282865 | 0.520753742 | 9.871731751 |
| MC_MAL_1261_2.mat | 0.169100619 | 0.045251288 | 0.560550804 | 10.27402574 |
| MC_MAL_1489_3.mat | 0.263603928 | 0.056305188 | 0.497930208 | 8.601244908 |
| MC_MAL_1489_3.mat | 0.281680512 | 0.104564151 | 0.471713332 | 8.635614903 |
| MC_MAL_1489_3.mat | 0.526367163 | 0.152104016 | 0.457677954 | 6.804866281 |
| MC_MAL_1500_4.mat | 0.116269126 | 0.080335843 | 0.537378749 | 10.50014809 |
| MC_MAL_1500_4.mat | 0.456465467 | 0.161559187 | 0.490870772 | 8.679624401 |
| MC_MAL_1500_4.mat | 0.0748728 | 0.07290368 | 0.577239013 | 9.202154937 |
| MC_MAL_1500_4.mat | 0.254405515 | 0.093711326 | 0.414603428 | 4.981200977 |
| MC_MAL_1528_3.mat | 0.18436958 | 0.070862081 | 0.402003621 | 4.324873083 |

Table C.1 – Continued

| DDSM case | α | Fourier | Moment | Compactness |
|---|---|---|---|---|
| MC_MAL_1528_3.mat | 0.306801029 | 0.058848948 | 0.409957973 | 4.200789478 |
| MC_MAL_1528_3.mat | 0.308611533 | 0.133404105 | 0.43596188 | 10.10027633 |
| MC_MAL_1531_3.mat | 0.319234481 | 0.087314144 | 0.51174632 | 10.82943995 |
| MC_MAL_1531_3.mat | 0.152708705 | 0.052453178 | 0.532407278 | 11.36568894 |
| MC_MAL_1531_3.mat | 0.078910016 | 0.052493624 | 0.584414918 | 13.04077846 |
| MC_MAL_1585_2.mat | 0.383554559 | 0.106952859 | 0.459923552 | 6.969219653 |
| MC_MAL_1585_2.mat | 0.237802545 | 0.045428447 | 0.505105518 | 9.935222955 |
| MC_MAL_1590_1.mat | 0.311934405 | 0.137503952 | 0.441563734 | 6.809559505 |
| MC_MAL_1596_3.mat | 0.184663726 | 0.047623899 | 0.486958923 | 7.068926005 |
| MC_MAL_1596_3.mat | 0.709381311 | 0.243929298 | 0.398863283 | 5.766166333 |
| MC_MAL_1596_3.mat | 0.122822974 | 0.047556711 | 0.532254288 | 9.638077571 |
| MC_MAL_1596_3.mat | 0.312693951 | 0.157515141 | 0.385302111 | 4.971933268 |
| MC_MAL_1614_1.mat | 0.279711636 | 0.185862161 | 0.391656876 | 2.370364398 |
| MC_MAL_1637_3.mat | 0.343815373 | 0.34637897 | 0.42792009 | 5.172230163 |
| MC_MAL_1637_3.mat | 0.111443195 | 0.129532409 | 0.447270004 | 6.331248349 |
| MC_MAL_1637_3.mat | 0.187388839 | 0.072121916 | 0.584937729 | 9.959543231 |
| MC_MAL_1675_1.mat | 0.453423306 | 0.296936482 | 0.400399786 | 6.102914113 |
| MC_MAL_1819_6.mat | 0.049790479 | 0.024865456 | 0.608561588 | 9.123623387 |
| MC_MAL_1819_6.mat | 0.268159321 | 0.095789079 | 0.549391041 | 7.730060595 |
| MC_MAL_1819_6.mat | 0.082978846 | 0.060576405 | 0.591204488 | 9.290962262 |
| MC_MAL_1819_6.mat | 0.096210538 | 0.033185264 | 0.636884397 | 11.00212499 |
| MC_MAL_1819_6.mat | 0.109517805 | 0.032407344 | 0.609691765 | 8.538077718 |
| MC_MAL_1819_6.mat | 0.239905213 | 0.083221267 | 0.522182459 | 10.20360406 |
| MC_MAL_1894_1.mat | 0.338617962 | 0.353741483 | 0.369843643 | 4.051984831 |
| MC_MAL_1897_5.mat | 0.293965363 | 0.102611262 | 0.557918215 | 9.152596853 |
| MC_MAL_1897_5.mat | 0.302933296 | 0.096897907 | 0.470096906 | 8.66638869 |
| MC_MAL_1897_5.mat | 0.315450765 | 0.095325874 | 0.417070176 | 6.616819331 |
| MC_MAL_1897_5.mat | 0.081683997 | 0.018059487 | 0.582050726 | 3.972919821 |
| MC_MAL_1897_5.mat | 0.163955992 | 0.049746699 | 0.573113051 | 6.893859386 |
| MC_MAL_1905_1.mat | 0.363717075 | 0.078664382 | 0.505186397 | 11.71062071 |
| MC_MAL_1907_2.mat | 0.084295431 | 0.021871202 | 0.57131448 | 6.179503044 |
| MC_MAL_1907_2.mat | 0.312295358 | 0.121419954 | 0.399893971 | 9.557157628 |
| MC_MAL_4151_5.mat | 0.157774791 | 0.118388393 | 0.558258221 | 9.230696185 |
| MC_MAL_4151_5.mat | 0.20612677 | 0.062788457 | 0.47223981 | 9.564674829 |

Table C.1 – Continued

| DDSM case | α | Fourier | Moment | Compactness |
|---|---|---|---|---|
| MC_MAL_4151_5.mat | 0.280896199 | 0.060216824 | 0.483313692 | 10.0384325 |
| MC_MAL_4151_5.mat | 0.10782223 | 0.060044194 | 0.57394912 | 8.446726407 |
| MC_MAL_4151_5.mat | 0.16972228 | 0.081322371 | 0.580107609 | 10.20379928 |
| MC_MAL_4117_2.mat | 0.252391081 | 0.027172212 | 0.427275323 | 4.72104505 |
| MC_MAL_4117_2.mat | 0.201221691 | 0.042755448 | 0.613683593 | 10.58656446 |
| MC_MAL_4158_1.mat | 0.272765728 | 0.188414977 | 0.393244502 | 4.642228102 |
| MC_MAL_4161_2.mat | 0.298070732 | 0.06641729 | 0.470328725 | 6.944532205 |
| MC_MAL_4161_2.mat | 0.539178946 | 0.081682414 | 0.531691923 | 8.6697808 |
| MC_MAL_4182_5.mat | 0.217062366 | 0.030990162 | 0.568507446 | 11.1376256 |
| MC_MAL_4182_5.mat | 0.346165367 | 0.077566573 | 0.409462604 | 5.743061337 |
| MC_MAL_4182_5.mat | 0.151828105 | 0.075565922 | 0.539607809 | 10.04242461 |
| MC_MAL_4182_5.mat | 0.280567924 | 0.07313492 | 0.512680973 | 8.846371331 |
| MC_MAL_4182_5.mat | 0.139014811 | 0.052322337 | 0.535740904 | 10.66775184 |
| MC_MAL_63_4.mat | 0.05078913 | 0.039441553 | 0.645653922 | 9.650091481 |
| MC_MAL_63_4.mat | 0.069732072 | 0.01350984 | 0.625159677 | 10.48653801 |
| MC_MAL_63_4.mat | 0.075639336 | 0.073502706 | 0.605787149 | 10.85134788 |
| MC_MAL_63_4.mat | 0.322387299 | 0.059693762 | 0.581634993 | 12.70595006 |
| MC_MAL_87_2.mat | 0.199702352 | 0.067467241 | 0.563289444 | 8.563738456 |
| MC_MAL_87_2.mat | 0.361577435 | 0.064740406 | 0.467311351 | 11.75524669 |
| MC_MAL_90_2.mat | 0.265606749 | 0.098405971 | 0.539460706 | 9.889550053 |
| MC_MAL_90_2.mat | 0.092386819 | 0.031623253 | 0.574672448 | 10.54962524 |
| MC_MAL_96_2.mat | 0.234687875 | 0.074800255 | 0.470739498 | 7.629193722 |
| MC_MAL_96_2.mat | 0.421763241 | 0.16296421 | 0.415408277 | 7.070163511 |
| MC_MAL_99_2.mat | 0.188015136 | 0.137714018 | 0.455260326 | 9.278270858 |
| MC_MAL_99_2.mat | 0.503667296 | 0.22729483 | 0.378263597 | 5.786918791 |
| MC_MAL_106_4.mat | 0.139996976 | 0.044309131 | 0.561431326 | 8.777875486 |
| MC_MAL_106_4.mat | 0.468983351 | 0.127951778 | 0.500079687 | 7.853323192 |
| MC_MAL_106_4.mat | 0.251099422 | 0.071029401 | 0.545608669 | 10.77008865 |
| MC_MAL_106_4.mat | 0.20445071 | 0.060898494 | 0.454290225 | 5.98186467 |
| MC_MAL_132_3.mat | 0.286655134 | 0.053970416 | 0.465514088 | 8.720718134 |
| MC_MAL_132_3.mat | 0.211367938 | 0.104350373 | 0.551084621 | 6.888984272 |
| MC_MAL_132_3.mat | 0.111090457 | 0.060799648 | 0.541949396 | 10.65605139 |
| MC_MAL_167_1.mat | 0.388661871 | 0.456851315 | 0.352259982 | 5.694313149 |
| MC_MAL_171_3.mat | 0.225700483 | 0.077972193 | 0.547883075 | 8.712827494 |

Table C.1 – Continued

| DDSM case | α | Fourier | Moment | Compactness |
|---|---|---|---|---|
| MC_MAL_171_3.mat | 0.318132475 | 0.040758229 | 0.449842812 | 8.596802359 |
| MC_MAL_171_3.mat | 0.117018416 | 0.028821597 | 0.480048164 | 5.989701789 |
| MC_MAL_309_3.mat | 0.388581978 | 0.05315112 | 0.439518347 | 8.969793882 |
| MC_MAL_309_3.mat | 0.562154695 | 0.412860179 | 0.370874682 | 6.272691358 |
| MC_MAL_309_3.mat | 0.294832544 | 0.050372997 | 0.470699246 | 9.346801831 |
| MC_MAL_3044_4.mat | 0.141011138 | 0.025996265 | 0.556078786 | 7.753603423 |
| MC_MAL_3044_4.mat | 0.200597901 | 0.018457294 | 0.53218646 | 9.261168864 |
| MC_MAL_3044_4.mat | 0.660521239 | 0.224964415 | 0.374617758 | 5.811162849 |
| MC_MAL_3044_4.mat | 0.459873521 | 0.153684258 | 0.345108553 | 5.196387849 |
| MC_MAL_3055_5.mat | 0.199965258 | 0.052269033 | 0.479480094 | 9.188225493 |
| MC_MAL_3055_5.mat | 0.578240001 | 0.315239301 | 0.38008487 | 5.001795599 |
| MC_MAL_3055_5.mat | 0.171023292 | 0.034932694 | 0.475983358 | 6.74570752 |
| MC_MAL_3055_5.mat | 0.073506484 | 0.026655601 | 0.501392043 | 8.025074095 |
| MC_MAL_3382_3.mat | 0.328638051 | 0.122335785 | 0.591837158 | 10.63397466 |
| MC_MAL_3382_3.mat | 0.165001562 | 0.036242978 | 0.597874045 | 11.4536211 |
| MC_MAL_3382_3.mat | 0.199396347 | 0.060705454 | 0.564609708 | 11.14205273 |
| MC_MAL_3389_2.mat | 0.109308743 | 0.042350634 | 0.626327556 | 9.9927393 |
| MC_MAL_3389_2.mat | 0.26012133 | 0.032001708 | 0.493259011 | 8.484919629 |
| MC_MAL_3406_2.mat | 0.357365892 | 0.084558158 | 0.436413 | 9.28687106 |
| MC_MAL_3406_2.mat | 0.213313147 | 0.100720388 | 0.567779043 | 7.325314436 |
| MC_MAL_3476_5.mat | 0.346551973 | 0.097383541 | 0.430315119 | 5.791465025 |
| MC_MAL_3476_5.mat | 0.364124272 | 0.098968699 | 0.421164515 | 6.995450454 |
| MC_MAL_3476_5.mat | 0.214231009 | 0.160554904 | 0.422500669 | 7.62657427 |
| MC_MAL_3476_5.mat | 0.246271404 | 0.114801648 | 0.389018979 | 4.873453616 |
| MC_MAL_3476_5.mat | 0.267247456 | 0.123192648 | 0.428715456 | 6.47474213 |
| MC_MAL_3498_2.mat | 0.290699714 | 0.091543027 | 0.41481946 | 10.65937887 |
| MC_MAL_3498_2.mat | 0.238030455 | 0.085037123 | 0.401910364 | 4.749914547 |
| MC_MAL_3504_2.mat | 0.472145662 | 0.162701336 | 0.504748288 | 9.841025799 |
| MC_MAL_3504_2.mat | 0.151620411 | 0.065511853 | 0.578661906 | 12.03739035 |
| MC_MAL_3512_5.mat | 0.089739537 | 0.01109452 | 0.632236507 | 10.01128331 |
| MC_MAL_3512_5.mat | 0.194881775 | 0.068226344 | 0.472766946 | 7.527378041 |
| MC_MAL_3512_5.mat | 0.54132829 | 0.108928591 | 0.458065648 | 12.42070913 |
| MC_MAL_3512_5.mat | 0.227827526 | 0.037475408 | 0.473564387 | 7.832895435 |

# BIBLIOGRAPHY


[1] H. Soltanian-Zadeh, F. Rafiee-Rad, and S. Pourabdollah-Nejad D, "Comparison of multiwavelet, wavelet, haralick, and shape features for microcalcification classification in mammograms," *Pattern Recognition*, vol. 37, no. 10, pp. 1973 – 1986, 2004.

[2] "Deaths: Final data for 2006," *National Vital Statistics Reports*, vol. 57, no. 14, pp. 1 – 135, 2009.

[3] "Breast cancer facts & figures 2009-2010," http://www.cancer.org/downloads/STT/F861009_final%209-08-09.pdf, 2009 (accessed Feb 6, 2010).

[4] "Breast cancer: Early detection," http://www.cancer.org/docroot/CRI/content/CRI_2_6x_Breast_Cancer_Early_Detection.asp, 2009 (accessed Feb 6, 2010).

[5] E. A. Sickles, "Breast calcifications: Mammographic evaluation," *Radiology*, vol. 160, pp. 289–293, 1986.

[6] H. D. Cheng, X. Cai, X. Chen, L. Hu, and X. Lou, "Computer-aided detection and classification of microcalcifications in mammograms: a survey," *Pattern Recognition*, vol. 36, no. 12, pp. 2967 – 2991, 2003.

[7] F. Lefebvre, H. Benali, E. Kahn, and R.D. Paola, "A fractal approach tothe segmentation of microcalcifications in digital mammograms," *Med.Phys.*, vol. 22, no. 4, pp. 381–391, 1995.

[8] N. S. Arikidis, A. Karahaliou, S. Skiadopoulos, P.s Korfiatis, E. Likaki, G. Panayiotakis, and L. Costaridou, "Size-adapted microcalcification segmentation in mammography utilizing scale-space signatures," *Computerized Medical Imaging and Graphics*, vol. In Press, Corrected Proof, pp. –, 2010.

[9] L. P. Clarke, M. Kallergi, W. Qian, H. Li, R. A. Clark, and S. M. L., "Tree-structured non-linear filter and wavelet transform for microcalcification segmentation in digital mammography," *Cancer Letters*, vol. 77, no. 2-3, pp. 173 – 181, 1994, Computer applications for early detection and staging of cancer.

[10] B. Liu, H.D. Cheng, J. Huang, J. Tian, J. Liu, and X. Tang, "Automated segmentation of ultrasonic breast lesions using statistical texture classification and active contour based on probability distance," *Ultrasound in Medicine & Biology*, vol. 35, no. 8, pp. 1309 – 1324, 2009.

[11] A. Papadopoulos, D. I. Fotiadis, and A. Likas, "An automatic microcalcification detection system based on a hybrid neural network classifier," *Artificial Intelligence in Medicine*, vol. 25, no. 2, pp. 149 – 167, 2002.

[12] M. G. Linguraru, K. Marias, R. English, and M. Brady, "A biologically inspired algorithm for microcalcification cluster detection," *Medical Image Analysis*, vol. 10, no. 6, pp. 850 – 862, 2006.

[13] A. Papadopoulos, D.I. Fotiadis, and L. Costaridou, "Improvement of microcalcification cluster detection in mammography utilizing image enhancement techniques," *Computers in Biology and Medicine*, vol. 38, no. 10, pp. 1045 – 1055, 2008.

[14] N.a Ahuja, A. Rosenfeld, and R. M. Haralick, "Neighbor gray levels as features in pixel classification," *Pattern Recognition*, vol. 12, no. 4, pp. 251 – 260, 1980.

[15] R. M. Haralick, "Statistical and structural approaches to texture," *Proc. IEEE*, vol. 67, no. 5, pp. 786 – 804, 1979.

[16] J.Y. Tham, L.X. Shen, S.L. Lee, and H.H. Tan, "A general approach for analysis and application of discrete multiwavelet transforms," *Signal Processing*, vol. 48, no. 2, pp. 457 – 464, 2000.

[17] S. Yu, K. Li, and Y. Huang, "Detection of microcallcification in digital mammograms using wavelet filter and markov random field model," *Computerized Medical Imaging and Graphics*, vol. 30, pp. 163 – 173, 2006.

[18] L. Shen, R. M. Rangayyan, and J. E. L. Desautels, "Application of shape analysis to mammographic calcifications," *IEEE Trans. Med. Imag.*, vol. 13, no. 2, pp. 263–274, June 1994.

[19] C. Xu and J. L. Prince, "Snakes, shapes, and gradient vector flow," *IEEE Trans. Image Processing*, vol. 7, no. 3, pp. 359–369, March 1998.

[20] M. Kass, A. Witkin, and D. Terzopoulos, "Snakes: Active contour models," *Int. J. Comput. Vis.*, vol. 1, pp. 321 – 331, 1987.

[21] R. C. Gonzalez and R. E. Woods, *Digital Image Processing*, Prentice Hall, Upper Saddle River, New Jersey 07458, second edition, 2002.

[22] T. Fawcett, "An introduction to roc analysis," *Pattern Recognition Letters*, vol. 27, no. 8, pp. 861 – 874, 2006, ROC Analysis in Pattern Recognition.